AEDC-TR-94-13

Kinematic Telemetry from Small-Scale Wind Tunnel Models

E. J. Marquart, K. I. Davis, G. P. Walker, F. J. Gamble, and R. E. Dix
Micro Craft Technology/AEDC Operations

May 1995

Final Report for Period October 1992 — September 1994

ARNOLD ENGINEERING DEVELOPMENT CENTER
ARNOLD AIR FORCE BASE, TENNESSEE
AIR FORCE MATERIEL COMMAND
UNITED STATES AIR FORCE

NOTICES

When U. S. Government drawings, specifications, or other data are used for any purpose other than a definitely related Government procurement operation, the Government thereby incurs no responsibility nor any obligation whatsoever, and the fact that the Government may have formulated, furnished, or in any way supplied the said drawings, specifications, or other data, is not to be regarded by implication or otherwise, or in any manner licensing the holder or any other person or corporation, or conveying any rights or permission to manufacture, use, or sell any patented invention that may in any way be related thereto.

Qualified users may obtain copies of this report from the Defense Technical Information Center.

References to named commercial products in this report are not to be considered in any sense as an endorsement of the product by the United States Air Force or the Government.

This report has been reviewed by the Office of Public Affairs (PA) and is releasable to the National Technical Information Service (NTIS). At NTIS, it will be available to the general public, including foreign nations.

APPROVAL STATEMENT

This report has been reviewed and approved.

DANIEL MAGEE, Capt, CF
Propulsion Technology
Applied Technology Division
Test Operations Directorate

Approved for publication:

FOR THE COMMANDER

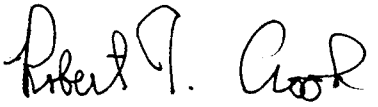

ROBERT T. CROOK
Asst Chief, Applied Technology Division
Test Operations Directorate

REPORT DOCUMENTATION PAGE

Form Approved
OMB No. 0704-0188

1. AGENCY USE ONLY (Leave blank)	2. REPORT DATE	3. REPORT TYPE AND DATES COVERED
	May 1995	Final Report for Period October 1992 - September 1994

4. TITLE AND SUBTITLE

Kinematic Telemetry from Small-Scale Wind Tunnel Models

5. FUNDING NUMBERS

PN - 0110

6. AUTHOR(S)

Marquart, E.J., Davis, K.I., Walker, G.P., Gamble, F.J., and Dix, R.E., Micro Craft Technology/AEDC Operations

7. PERFORMING ORGANIZATION NAME(S) AND ADDRESS(ES)

Arnold Engineering Development Center/DOT
Air Force Materiel Command
Arnold Air Force Base, TN 37389-9011

8. PERFORMING ORGANIZATION (REPORT NUMBER)

AEDC-TR-94-13

9. SPONSORING/MONITORING AGENCY NAMES(S) AND ADDRESS(ES)

Arnold Engineering Development Center/DOT
Air Force Materiel Command
Arnold Air Force Base, TN 37389-9011

10. SPONSORING/MONITORING AGENCY REPORT NUMBER

11. SUPPLEMENTARY NOTES

Available in Defense Technical Information Center (DTIC).

12A. DISTRIBUTION/AVAILABILITY STATEMENT

Approved for public release; distribution is unlimited.

12B. DISTRIBUTION CODE

13. ABSTRACT (Maximum 200 words)

The development, assembly, calibration, and testing of a kinematic telemetry technique of determining the trajectory of a small model in free motion in a wind tunnel is described. Instead of measuring model displacement from a film record of the trajectory, accelerations of the model in the conventional six degrees of freedom were determined through the use of accelerometers and solid-state telemetry. Four models of a 1/15-scale fuel tank were each equipped with six linear accelerometers and one velocity sensor, analog-to-digital converters, and an eight-channel transmitter, all powered by a lithium battery pack.The models were released at transonic conditions in the wind tunnel. Model acceleration data were transmitted to a receiver and decoder outside the tunnel. The decoded digital data were stored on a personal computer equipped with a 32-bit data acquisition card and custom software. Correlation of accelerometer-based trajectories with conventional photography-based trajectories was good to excellent.

14. SUBJECT TERMS	15. NUMBER OF PAGES
telemetry, kinematic telemetry, trajectories, wind tunnel testing	66
	16. PRICE CODE

17. SECURITY CLASSIFICATION OF REPORT	18. SECURITY CLASSIFICATION OF THIS PAGE	19. SECURITY CLASSIFICATION OF ABSTRACT	20. LIMITATION OF ABSTRACT
UNCLASSIFIED	UNCLASSIFIED	UNCLASSIFIED	SAME AS REPORT

PREFACE

The work reported herein was done at the Arnold Engineering Development Center (AEDC), Air Force Materiel Command (AFMC), Arnold Air Force Base, TN, at the request of the AEDC Directorate of Technology (DOT). Applied technology work was done by Micro Craft Technology, support contractor for the aerospace flight dynamics test facilities at AEDC. The technology effort was completed as part of AEDC Project Number 0110, with Captain (CF) Dan Magee, AEDC/DOT as Air Force Project Manager. Work was accomplished during the period October 1992 through September 1994, and the manuscript was submitted for publication on April 11, 1995.

CONTENTS

ILLUSTRATIONS

Figure Page

APPENDIX

1.0 INTRODUCTION

Ground test simulation of moving bodies is usually performed with scaled models of the actual body. This is certainly the case in wind tunnel simulations of flight vehicles, where a popular method of studying the motion of stores separating from aircraft, i.e., the Captive Trajectory Support System (CTS), often involves the use of small models (one-twentieth of full size is common). Ordinarily, CTS testing involves an aircraft model that is supported rigidly in the test section, with the separating store model mounted on a strain-gage balance supported by a totally independent sting. The trajectory of the store model is then generated by moving the store model to positions relative to the aircraft model that are predicted on the basis of the aerodynamic forces and moments sensed by the strain-gage balance on which the store model is mounted (Ref. 1). In the case of a light, active store such as an empty fuel tank (large volume, low mass), store motions can become violent, with large amplitude displacements occurring at high rates. In these cases, as it attempts to move the store model along the predicted path, the CTS system could easily be driven to the travel limits of the mechanism, and the store model sting could be forced into a collision with the aircraft model, causing a premature termination of the test. The alternative method of simulating the trajectory is the free-drop or dynamic-drop method, in which the store model is simply released or ejected from the aircraft model, falling freely away into the wind tunnel free stream. Two mutually orthogonal cameras are used to make a record of the spatial trajectory on film. Later, displacements of identified points on the model are tracked visually and measured from the film using a projector capable of projecting a frame-by-frame image. A superimposed cursor provides a means of transmitting the coordinates of the identified point to a computer (Refs. 2–3).

Until now, the film or video record has been the standard means of providing a spatial description of the trajectory of a freely moving body. Unfortunately, because of the time required to develop the film and perform the frame-by-frame analysis, lengthy delays between the test and the availability of the trajectory for analysis have also become standard. When the trajectory parameters have finally been deduced, they are quoted with relatively high degrees of uncertainty, because of the difficulty of tracking points on film or video tape of inadequate resolution. Furthermore, it has not been possible to extract from film records accurate estimates of the forces and moments acting on the freely moving body. A search for an alternate method of distilling the trajectory from a free-drop simulation while simultaneously decreasing the time delay and improving accuracy led to consideration of kinematic telemetry. Telemetry had been considered previously but eliminated because of the large size and mass of available components. Recent decreases, however, in both the size and power requirements of accelerometers have once again stimulated interest in full six degree-of-freedom (6-DOF) kinematic measurement and telemetry systems that are small enough to have practical application in small-scale wind tunnel models. After considerable market research, it was decided to attempt development of a kinematic accelerometer and telemetry module (KTM) that could be mounted totally within a small-scale free-drop store

model and provide direct sensing of the accelerations of the moving model. Given the extremely fast response times of the available accelerometers, it was noted that an additional significant advantage of the technique would be the sensing (albeit indirectly) of the fluctuating loads acting on a body without the magnitude and frequency-response limits imposed by the physical and inertial properties of conventional static-force instrumentation, i.e., strain-gage balances.

The telemetry system developed at the AEDC is capable of sensing and transmitting full 6-DOF kinematic acceleration data from a moving body. Totally enclosed in a model, the KTM module comprises batteries, accelerometers that are, effectively, small transducers that produce voltage levels proportional to kinematic acceleration and rate, analog-to-digital (A/D) converters, and a multi-channel Ultra-High Frequency (UHF) transmitter and antenna. Digitized and encoded acceleration data are transmitted from inside the freely moving model at 10,000 channel-samples/sec using 16-bit simultaneous-sample-and-hold instrumentation packages weighing less than 8 oz and occupying less than 5 cubic inches. A nearby receiver system decodes the bit stream and passes the data directly into the random access memory (RAM) of a personal computer. At a convenient time after the model is dropped, the acceleration data are transferred to a hard disk and reduced to engineering units for analysis purposes. The forces and moments acting on the moving model are calculated from the kinematic measurements and from the mass and moment of inertia properties of the model.

A numerical simulation study was performed to evaluate various methods of kinematic telemetry measurements, and the predicted accuracy of such a measurement scheme was shown to be far better than that attainable using high-speed photography (Ref. 4). A description is included here of the use of kinematic telemetry at the AEDC, concentrating on the initial development of the telemetry instrumentation for free-motion testing in wind tunnels. The technology, while being developed for the wind tunnels, will also have direct application in gun ranges and space chambers.

2.0 TWO METHODS OF MOTION ANALYSIS

2.1 PHOTOGRAPHIC METHODOLOGY

It is conventional to record the motion of a freely falling store model in a wind tunnel test on film exposed at a rate of 400 frames per sec. Two cameras are used, one mounted on the floor and the other on one side wall of the wind tunnel test section, respectively, thereby capturing images in two mutually orthogonal fields of view. Figure 1 is an illustration of a frame of a typical film record.

Spatial position and attitude of the model are determined by tracking from frame-to-frame the movement of three identified points–usually a point at the extreme upstream extent of the model (the nose), a point at the extreme downstream extent of the model (the tail), and a point off the

longitudinal axis of the model, such as the tip of a control surface, or fin. Linear and angular displacements in the longitudinal and lateral planes are determined by measuring the movement of the identified points at the nose and tail of the model relative to a calibrating grid marked on a board that is mounted in the test section and filmed prior to the test. The off-axis point is used to determine angular displacement in the roll degree of freedom.

The process of recording the coordinates of a point on the film involves projecting a frame of the film on a rear-projection screen, placing the intersection of two mutually orthogonal thin wires over the point to be identified, and pressing a button. The coordinates of the point, corresponding to the position of the wires, are transmitted directly to a computer, where the values are compiled and used in equations that yield a digital description of the 6-DOF trajectory of the model. Although machines are involved in recording and calculating the trajectory, the process of locating the identified control points in each frame is manual, i.e., the film operator must display the frame on the screen of a workstation and choose where to place the cursor. (The photographic method is described completely in Refs. 2 and 3.) Consequently, when defining the accuracy of trajectories deduced from the photograhic record of a drop, not only must the resolution of the film be considered, but also estimates of the ability of the human to consistently identify the control points in a frame. In general, the mathematical model used to describe the process of making a measurement is constructed by combining estimates of two common sources of error, i.e., bias and random error. The bias component is selected to account for any constant offset (e.g., an incorrect tare weight, or in the case of a film record, the parallax associated with a fixed camera position), while the random error accounts for the statistical spread of values of repeated measurements of the same quantity (e.g., the location of a control point within a blurred image on the film). The random error component is assumed to be the domain of ± two standard deviations, which would include 95 percent of all measurement samples, assuming sample sizes of 30 or more. Combining these considerations, the uncertainties associated with film reading are:

Measure	Quoted Uncertainty (at model)
Linear Displacements	± 0.5 in. (average of X, Y, and Z)
Pitch and Yaw Angles	± 2 deg
Roll Angles	± 20 deg

2.2 ACCELEROMETER METHODOLOGY

2.2.1 Selection of an Accelerometer Technique

Accelerometer methodology involves the use of transducers capable of sensing linear acceleration, angular acceleration, or angular velocity (angular rate). These components may be

combined in several different ways to sense the acceleration of a freely moving body in the conventional six degrees of freedom. Of the various techniques of implementing accelerometer methodology, three were considered, differing in type and location of the transducers used, and described as follows:

1. Indirect sensing of linear and angular acceleration, using a tri-axial accelerometer and three angular accelerometers ("acceleration" technique);

2. Direct sensing of linear acceleration and angular rate, using single-axis accelerometers and rate gyros ("acceleration/rate" technique); and

3. Direct sensing of both linear and angular acceleration, using single-axis accelerometers ("linear/linear" technique).

In all cases, the planned mode of operation was to convert the analog acceleration data from the transducers in the body to engineering units of acceleration (A to D conversion), transmit the digital data to a receiver adjacent to the wind tunnel test section, and transfer (not telemeter) the data to a workstation or personal computer for mathematical integration in an appropriate set of equations to provide the conventional 6-DOF velocities and displacements. Sketches illustrating possible arrangements of the components in a typical store model are shown in Fig. 2.

2.2.2 Comparison of Accelerometer Techniques – Numerical Simulation of a Trial Case

An assessment of the capability afforded by each technique was made using a hypothetical trial case. An aircraft fuel tank was selected as the store model, partly because the free-drop technique of evaluating store motion upon release is often used for fuel tanks, and partly because scaled models of fuel tanks are usually large compared with other store configurations, providing adequate internal volume in which to mount the accelerometer and telemetry circuit components.

Separation of the tank was assumed, for simplicity, to take place in a vacuum. A motion consisting of only vertical translation and pitching was assumed. Comparisons were made between body motions that could be deduced from integrations of the accelerometer data, and motions that could be extracted from the photographic method (described in Section 2.0) of conventional frame-by-frame reading of film records of the moving-body scene.

Using the quoted position uncertainty of ± 0.5 in. for photographic data reduction, and assuming film reading errors could be represented by a Gaussian distribution, the photographic method applied to the simple 1-g release in a vacuum yielded a time-history of the vertical position of the center of gravity of the model as depicted in Fig. 3a. The time history of the pitch degree of

freedom was calculated in a similar fashion and is illustrated in Fig. 3b, assuming a rotation rate of 4 rad/sec in the XZ plane and again applying the quoted ±2-deg uncertainty.

The linear acceleration of the model in the vertical (Z) direction during the trajectory was calculated as the second derivative with respect to time of the Z-position history as determined using the simulated photographic measurements. First and second derivatives were calculated from the folowing equations, using the sequential points of displacements in the vertical (Z) direction illustrated in Fig. 3a:

$$\dot{Z}_t = \frac{Z_{t+\Delta t} - Z_{t-\Delta t}}{2\Delta t} \tag{1}$$

$$\ddot{Z}_t = \frac{\dot{Z}_{t+\Delta t} - \dot{Z}_{t-\Delta t}}{2\Delta t} \tag{2}$$

Because film of free-drop sequences is normally exposed at 400 frames/sec, then $\Delta t = 0.0025$ sec. The calculated linear accelerations are illustrated as the graph shown in Fig. 4a, showing that errors of approximately 100 g are clearly possible.

Angular accelerations of the model in the pitch (XZ) plane were calculated in a similar manner, using the calculated pitch angles of Fig. 3b in the following equations:

$$\dot{\theta}_t = \frac{\theta_{t+\Delta t} - \theta_{t-\Delta t}}{2\Delta t} \tag{3}$$

$$\ddot{\theta}_t = \frac{\dot{\theta}_{t+\Delta t} - \dot{\theta}_{t-\Delta t}}{2\Delta t} \tag{4}$$

As for the Z DOF calculations, $\Delta t = 0.0025$ sec. The calculated angular accelerations in the pitch plane are illustrated as the graph shown in Fig. 4b, again showing that large errors are possible when using the photographic method – on the order of 5,000 rad/sec^2.

Finally, it is clear that, although calculated accelerations could be used to infer forces and moments acting on the model, the large uncertainties concomitant with such a process would make it difficult to extract meaningful data. The primary use, then, of photographic records of freely moving models in the wind tunnel is to provide a visual image of events that occur at eye-blink rates – an image that can be replayed at will and at speeds that allow for human comprehension and qualitative evaluation. Position and attitude trajectories can be extracted with reasonable accuracy, but manipulation of the distance-time information by mathematics to provide related characteristics, such as forces and moments, is marked by high uncertainty.

2.2.3 The "Acceleration" Technique

Using linear and angular acceleration transducers, both linear and angular acceleration can be sensed directly, substituted in equations that are integrated twice to calculate position and attitude. As indicated in Fig. 2a, associated instrumentation would include an A/D converter, a transmitter circuit, one tri-axial accelerometer, and three angular accelerometers.

It is assumed that for the trial case, the 1-g linear acceleration in the Z direction can be sensed by the tri-axial accelerometer and recorded with an uncertainty of ±3 percent, comprised of a ±1-percent bias and a ±2-percent precision error (approximately two standard deviations). Hypothetical acceleration data in the vertical (Z) direction of the model are illustrated in Fig. 5a, and can be compared there with corresponding data calculated from integrations of photographic records (copied from Fig. 3a). Directly sensed accelerations yield data that are characterized by uncertainties several orders of magnitude less than the uncertainties associated with the photographic method. Furthermore, acceleration data can be sensed at very high rates of 10,000 samples/sec or more, or 25 times as often as the 400 frames/sec of photographic data. As a result, a very detailed description of the process under study can be recorded, providing far better understanding of the process than with photographic methods.

In the pitch degree of freedom, it is assumed that the trial case pitching acceleration can be sensed to an uncertainty of about ± 0.15 rad/sec^2, comprised of a bias of 0.05 rad/sec^2 and a precision of two standard deviations, or ± 0.10 rad/sec^2. Comparison of the directly sensed hypothetical pitch acceleration and the pitch acceleration calculated from photographic records (copied from Fig. 3b) can be made in Fig. 5b. Angular acceleration by sensor is clearly superior to angular acceleration calculated by differentiation of data from photographic sources.

2.2.4 The "Acceleration/Rate" Technique

Transducers can be acquired to sense angular rate instead of angular acceleration, and a typical installation of three angular rate transducers and one tri-axial linear accelerometer would resemble the sketch of Fig. 2b. It is assumed that the imposed angular velocity of 4 π rad/sec can be sensed with an uncertainty of approximately 0.1 rad/sec, comprised of a two-standard-deviation precision error of ±0.07 rad/sec, and a bias error of ±0.03 rad/sec. Because linear acceleration is sensed with the same tri-axial accelerometer as in the "acceleration method," it is again assumed that for the trial case, the 1-g linear acceleration in the Z direction can be sensed and recorded with an uncertainty of ±3 percent, comprised of a ±1-percent bias and a two-standard-deviation (±2-percent) precision error. The assumed acceleration data in the vertical (Z) direction of the model are illustrated in Fig. 6a, together with corresponding data calculated from integrations of photographic records (copied from Fig. 3a).

In the pitch degree of freedom, pitch accelerations are calculated by differentiation of the angular rate (velocity) data using Eq. (4) with $\Delta t = 0.0001$ sec. It is assumed that the trial case pitching acceleration can be sensed to the same degree of certainty as in the acceleration case, i.e., a total uncertainty of about ± 0.15 rad/sec^2, comprised of a bias of 0.05 rad/sec^2 and a precision uncertainty of two standard deviations, or ± 0.10 rad/sec^2. Comparison of the calculated pitch acceleration and the pitch acceleration deduced from photographic records (copied from Fig. 3b) can be made in Fig. 6b. Despite the exaggeration of precision errors by mathematical differentiation, angular acceleration determined from an angular rate sensor in the "acceleration/rate technique" is superior to angular acceleration calculated from photographic sources.

2.2.5 The "Linear/Linear" Technique

Two tri-axial accelerometers are required in the "linear/linear" technique, one mounted well forward in the model, and one mounted well aft. In such a configuration, accelerations in the pitch (XZ) and yaw (XY) planes can be sensed with good resolution. An angular rate sensor must be used to sense rolling motion, because almost all of the store models in which the accelerometer/telemetry technique would be used are slender. (Two linear accelerometers could be mounted diametrically opposed about the longitudinal axis of the body, but the accelerometers must be mounted with significant separation to attain sufficient resolution of the rolling moment. Typical store configurations provide inadequate width for such side-by-side mounting of linear accelerometers.) A typical "linear/linear" installation is illustrated in Fig. 2c.

With two linear transducers sensing linear motion, the acceleration in a given direction can be calculated – e.g., in the manner of the simple numerical study – as the simple average of the two, or

$$\ddot{Z}_1 = \frac{\ddot{Z}_{1,\,Forward} - \ddot{Z}_{1,\,Rear}}{2} \tag{5}$$

Just as for the "acceleration" technique, it is assumed that the trial-case 1-g linear acceleration in the Z direction could be sensed by the tri-axial accelerometer and recorded with an accuracy of ± 3 percent, comprised of a ± 1-percent bias and a ± 2-percent precision error (approximately two standard deviations). Acceleration data in the (Z) direction of the model are the same as those of the acceleration/rate technique illustrated in Fig. 6a, and are not repeated.

In the pitch degree of freedom, pitch accelerations are calculated from the difference in the forward and aft accelerations divided by the distance between the transducers, or

$$\ddot{\theta} = \frac{\ddot{Z}_{Forward} - \ddot{Z}_{Rear}}{x_Z} \tag{6}$$

Because only linear accelerometers are involved, the uncertainty assumed for the "accelerometer" case applies, i.e., an uncertainty of ± 3 percent, comprised of a ± 1-percent bias and a ± 2-percent precision error (approximately two standard deviations). Comparison of the calculated hypothetical pitch acceleration and the pitch acceleration calculated from photographic records (copied from Fig. 3b) can be made in Fig. 6b. Once again the uncertainty of pitch acceleration determined from accelerometers is many times less than the uncertainty determined from photographic methods.

Attitude of the body is determined by twice integrating the net acceleration in the Z direction with respect to time. Model attitude for the trial case is illustrated in Fig. 7, where the attitude error is approximately 1 deg after 0.25 sec, and 3 deg after 0.4 sec, which is the extent of most free-drop trajectories in a small wind tunnel. Note that the uncertainty of the attitude result is worst when the bias errors of the two tri-axial accelerometers are opposite in sign. Precision errors, however, are minimized by the integration process, attested to by the coherent nature of the data illustrated in Fig. 7.

2.2.6 Summary of Techniques and Final Selection

The uncertainties expected with the acceleration techniques considered and the uncertainty associated with the photographic method can be compared in the following table:

	Uncertainty			
Technique	Linear Acceleration, g	Angular Acceleration, rad/sec^2	Position, in.	Attitude, deg
Photographic	± 100	± 5,000	± 0.30	± 2
Acceleration	± 0.05	± 0.25	± 0.25	± 0.2
Acceleration/Rate	± 0.05	± 100	± 0.25	± 0.7
Linear/Linear	± 0.05	± 2	± 0.25	± 3

Substantial decreases in the uncertainty of model accelerations are evident, of course, when using either of the accelerometer techniques, a fact attributable to the effects of amplification of approximations by differentiation of data derived from photographs. Because the determination of the position of the body using accelerometers involves mathematical integration of directly sensed digital data, the smoothing effect of the integration process produces position information with about the same degree of certainty (or uncertainty) as directly measured data from photographs. Likewise, model attitude can be stated to within one order of magnitude of the same certainty using either of the techniques.

With regard to final selection of a technique to use, it was clear that either the acccceleration technique or the linear/linear technique would yield results of about the same certainty. (The acceleration/rate technique was eliminated because of the high uncertainty of angular accelerations associated with mathematical differentiation of data from angular rate transducers.) Angular accelerometers are bulky and fragile, hence the acceleration technique was rejected. Therefore, by elimination, the linear/linear technique was selected as the best choice for evaluating a kinematic accelerometer and telemetry module (KTM).

3.0 KTM EVALUATION IN A WIND TUNNEL TEST

3.1 WIND TUNNEL

Performance of a KTM-equipped fuel tank was evaluated during a test in the AEDC Aerodynamic Wind Tunnel 4T, a closed-circuit tunnel in which continuous flow can be maintained at various values of free-stream density. Using the two flexible opposite walls of the two-dimensional nozzle, appropriate nozzle contours can be set to provide values of Mach number in the free stream at any value from 0.1 to 2.00. Stagnation pressure can be maintained at any value from 300 to 3,700 psfa, while stagnation temperature can be maintained from 550 to 580°R. The test section is 4 ft square and 12.5 ft long, with perforated walls. Wall porosity can be varied from 0.5- to 10-percent open. During testing, the effects of blockage and shock reflection can be reduced by suction of a portion of the airflow from the test section through the porous walls into a plenum chamber enveloping the test section.

Tests involving releases of a model into the flow to study the motions of the freely falling body naturally involve attaching the model to a releasing mechanism at a location near the ceiling of the test section. Often the mechanism is enclosed inside an aircraft model or attached to a pylon. A sketch of the Tunnel 4T test section with a typical installation of a model for Captive Trajectory Support system (CTS) testing is illustrated in Fig. 8. During free-drop testing, the aircraft sting support is removed, the pitch sector is retracted, and the CTS mechanism is removed. The aircraft (or other "parent" body) is then mounted as near the test section ceiling as possible. A photograph of a typical installation, including the model-catch net stretching across the lower portion of the test section, comprises Fig. 9. At this point, it is appropriate to point out that the subject of this document is the development of a kinetic telemetry module (KTM), and it is beyond the intended scope to describe in detail either the free-drop technique or the actual test in which KTM-equipped models were released. A complete textual description of the free-drop technique has been published in Refs. 2 and 3, and a description of the KTM evaluation test has been published in Ref. 5.

3.2 MODEL CONFIGURATION

Because of the likelihood of an active trajectory with significant displacements upon release, an aircraft fuel tank was selected as an appropriate configuration for a proof-of-principle test of a

KTM-equipped model in a wind tunnel experiment. It was recognized, of course, that in addition to reduced size and shape, appropriate scaling of the mass, center-of-gravity, and inertial characteristics of the full-size tank would be necessary to assure not only geometric similitude, but also kinematic similitude. Therefore, to provide a significant design challenge, an empty tank was selected, imposing stringent controls on the weight and cg location of the KTM to be inserted into the model. Both the shape and the dimensions of the tank are illustrated in Fig. 10. Specifications of the mass and inertial characteristics of the tank model were based on heavy-model scaling principles (Refs. 2 and 3). The tank model was fabricated by the Lockheed Fort Worth Company (LFWC) in Fort Worth, TX, using a thermo-plastic resin hardened into the desired shape with a laser-driven stereolithography technique (Ref. 5). Departing from conventional free-drop model fabrication practice, the model was made as a shell with the correct external shape. Within the model, reference surfaces and mounting guides were provided so that the KTM module could be firmly attached in a known location. When the model was completed, LFWC determined its mass, cg location, and inertial properties as follows:

Parameter	Model Value (2% Full 600-gal Tank + Pylon)	
W	1.812	lb
I_{XX}	2.290	lb-in.^{2}
I_{YY}	18.122	lb-in.^{2}
I_{ZZ}	16.580	lb-in.^{2}
X_{cg}	9.688	in.
Y_{cg}	0	in.
Z_{cg}	- 0.710	(Z is + down)
L	16.369	in.
$\dot{\theta}_m$	-644.4	deg/sec

4.0 KTM INSTRUMENTATION

4.1 ACCELERATION AND VELOCITY SENSORS

Accelerations in the six degrees of freedom of body motion were to be sensed with seven sensors, six accelerometers, and one roll sensor. The six linear accelerometers were attached to the mutually-perpendicular facets of two cubic blocks, forming tri-axial accelerometer units. The two tri-axial accelerometers were installed in forward and aft locations, respectively, to directly sense body acceleration in the conventional three degrees of translational freedom, and, knowing the relative location of the sensors and the body cg, the pitch and yaw degrees of freedom. Specifically,

the sensors were Endevco® model 7264-200 piezo-resistive accelerometers with a characteristic output of approximately 3 mv per g over a maximum range of 200 g. As with other resistive-style sensors, the accelerometers were designed for a DC excitation source, which was provided by using a ± 5-v supply that was made common to all sensors. The analog outputs of the accelerometers were limited by mechanical resonance effects to aproximaely 1,000 Hz.

Angular velocity in the roll degree of freedom was sensed using a magnetohydrodynamic device, model number ARS-04, manufactured by A. T. A. The sensor consisted of an induction coil surrounded by mercury suspended in a magnetic field. As the body rolled about its longitudinal axis, the output of the induction coil was recorded as mv/rad/sec. The coil output was proportional to the rolling velocity of the body, reversing in polarity as the direction of rolling motion reversed. Although an excitation voltage was not required, coil ouput was enhanced via an amplifier circuit supplied by unregulated power from a battery pack.

4.2 AMPLIFIERS

Amplification and signal conditioning were applied separately to the seven sensor channels, i.e., the six accelerometers and the roll velocity sensor. (No conditioning was needed for the eighth channel, the timing circuit.) Amplification was accomplished using amplifiers (Analog Devices Model AD797) which served not only to scale the maximum output of each sensor to the range of the A/D converters, but also to buffer the input to the converters while providing high slew rates and low-noise operation. Amplifiers were selected with a noise level specification of less than 0.0001525 v (equivalent to 1 least-significant bit of the 16-bit A/D converters) to avoid corrupting the digitized data signal.

Buffering the A/D input was accomplished by using the amplifiers in a non-inverting gain-type configuration, with the gain determined by the sensor output undergoing amplification. Consequently, it was necessary to spread the maximum output (e.g. ±200 g) over the ± 5-v range of the A/D converters. A single-pole low-pass filter was used to frequency-limit the noise and resonant components of the sensor output.

4.3 ANALOG-TO-DIGITAL (A/D) CONVERTERS

Converting the analog signal (a voltage) to a series of binary pulses for analysis as digital data was accomplished using an Analog Devices Model AD677, a self-calibrating, switched-capacitor input, successive-approximation converter. When a clock and sample pulse was applied to the A/D converter, a digital 16-bit word was created as an output. Each 16-bit word represented the sampled analog input every 100 μsec. The input range of measurement is ± 5 v over 65,536 possible counts. The output was provided in a serial Transistor-Transistor Logic (TTL) two's-complement format,

with the most significant bit first and ending with the least significant bit. Eighteen clock cycles were needed to complete one 16-bit word. The serial output was used to modulate the transmitter, and other outputs were used to control the logic and clock signals.

4.4 TIMING

Coordinated sampling of each A/D was enabled by use of a common clock signal generated by a quartz-crystal device oscillating at 6 MHz. The clock was pre-scaled by a factor of 32 to provide operation at 187,500 Hz, i.e., the frequency required to operate the A/D converters at the desired sample rate of 10,000 samples per sec (10 μsec between samples). In operation, the A/D converters issued a busy pulse as each word was transmitted. The busy pulse issued from a master A/D was used to initiate simultaneous operation of the other slave A/D converters. In operation, once started, the A/D converters continued to function until power was terminated, and the process could be resumed by simply reapplying power. It is worth noting that upon applying power, the A/D converters entered a self-calibrating mode and did not produce data for a minimum of 0.6 sec. The sample pulse used for recovery of the data clock was the eighth signal generated from the master busy signal, which was used at the receiver to reconstruct the clock and the beginning of a data word.

4.5. TRANSMITTER

A fundamental telemetry concept of providing a separate transmission frequency for each of the eight channels of information was implemented to simplify transmitter and receiver design. Selection of appropriate circuit components was thereby simplified because of the many personal communications networks that exist, providing a range of telemetry capabilities from cellular telephones to wireless personal computer communications. Specifically, a Motorola MC13176 transmitter chip was selected because of low power requirements and implementation flexibility. Using a single crystal and a few surface-mount passive components, the transmitter chip could provide oscillation over a frequency range of 250 to 1,000 MHz with the stability of a quartz crystal. Power output was adjustable to a maximum of +10 dBm, or 10 mw. A logic gate and a current-limiting resistor were used in the circuit with the transmitter chip to accomplish amplitude modulation (AM) of the radio-frequency (RF) carrier (also known as pulse-code modulation, or PCM). Signals were transmitted at frequencies selected to match the receivers, using a matched antenna connected to the RF output.

4.6. RECEIVER AND DECODER

Considerations of reliability, cost, and ease of implementation were paramount in the selection of a receiver. Because of the high data rate, a separate wide-band receiver with a base-band output was needed for each channel. Domestic cable television receiver subsystems were

known to offer inexpensive and readily available means of receiving data transmitted on carrier frequencies in the range from 57 to 885 MHz in 6-MHz increments. Consequently, a Scientific Atlanta Model 8540 cable receiver was used as the receiver, with a simple modification made to the detector circuit to route the video output signal to a decoder circuit.

Transmission frequencies were determined not only by the capability of the receiver, but also by the length of the model and the physical layout of the circuit board. Because of the need to enclose the transmitter antenna within the model, the antenna was limited to a quarter-wave-length, which defined a frequency range of from 300 to 500 MHz. Careful spacing of the eight frequencies in the available 200-MHz band was necessary to reduce co-channel interference. A single UHF aircraft antenna was mounted on the floor of the wind tunnel test section to receive the transmitted signals (Fig. 9).

The video output signal consisted of the data in serial format, so a decoder circuit had to be designed to detect and transform a level shift into a transistor-transistor-logic (TTL) signal. A two-stage limiter was used to reduce noise, and a comparator was used to detect the level. Data from all channels were sent to a bi-directional (I/O) card in the computer in serial form. Timing information was detected in the same way, but it was used to reset a clock circuit that matched the clock circuit in the model. A reset function realigned the clock at each sample pulse, maintaining timing and generating a clock function for the I/O card. In this way, a reduction was made in the information associated with transmission of the data, or "overhead." A total of 18 bits was used: 16 bits for the transmitted data plus two additional bits — one for the timing and one for the internal registers of the A/D converters. While this was not the most efficient use of RF and bitstream bandwidth, it was very easy to implement in the limited volume available in the model.

As illustrated in Fig. 11, only the framing pulse was above the level of the data. Following the trailing edge of the framing pulse, the next 16 clock cycles included the encoded accelerometer output, which was stored on a personal computer and converted to engineering-unit accelerations for ultimate use in other calculations.

4.7. DATA ACQUISITION

During the proof-of-concept test, a personal computer (PC) was used for data acquisition. The PC was a 66-MHz 486 with a 500-MB SCSI fixed disk and 12 MB of RAM. In addition, the PC was equipped with an EISA data bus and a National Instruments AT-DIO32F digital data acquisition (DDA) card. Custom software was written as a Microsoft Windows 3.1 application with Borland C++ version 3.0.

The DDA card was capable of recording up to 32 separate channels of digital information, separated into two 16-channel groups. An input and output handshake line was available for each of the two groups, although only one of "data-ready" line was used as the clock input from the receiver providing timing information to ensure synchronous data input. Each channel of data was sampled at a word rate of approximately 10 kHz. Data were transmitted in a serial mode, with each word comprised of 16 bits plus 1 overhead bit. Although each of the telemetry models had a slightly different internal clock, the data rate into the computer was approximately 180 kHz.

Data were stored in the PC as 16-bit integers. Eight bits of the integer consisted of output from the seven data channels plus one timing strobe channel. The remaining 8 bits were not used. Consequently, of each 16-bit integer stored by the computer, only one bit of each channel data word was represented, so that one bit from each of sixteen sequentially stored integers had to be combined to build each data word. If the data were viewed as a matrix, the computer stored the data as rows (16-bit integers), but the information for a given channel was contained in its respective bit column. Since relatively large amounts of data (2–3 MB) were stored in this manner for a few seconds of run time, an efficient method of transposing rows to columns was devised.

Converting each channel of digital data into usable information referenced to the accelerometer input was done in four steps. First, the data-ready input channel (the timing strobe) was isolated from all the other information, and the location and number of occurrences were noted as an indication of the number of data words. Second, the data channel of interest was isolated from the other channels (column information), and third, the value representing accelerometer output was determined. Finally, the information was presented in a graphical format on the computer screen. In the interest of computation speed, the first three steps were done with integer arithmetic. Much slower floating point arithmetic was involved in the final step of graphing the data, so when saving data to disk, only the first three steps were involved. Data were saved to disk rather than presented graphically.

5.0 BENCH CALIBRATION OF THE KTM

It was assumed, to preserve generality, that the installed orientation of each transducer in the model (the roll velocity sensor and each of the six linear accelerometers) was unique but unknown. Although each accelerometer was designed to be sensitive to accelerations in only one direction, the challenge was to determine that direction relative to the body axes of the model after the KTM was installed. Furthermore, just as fundamental to proper analysis of the acceleration data was knowledge of the mass and inertia properties of the model. An assessment of these crucial quantities was made by performing a bench-top calibration of the models after installation of the KTM, involving:

1. Dynamic verification of transducer operation;
2. Location and orientation of the six accelerometers relative to the model center of gravity; and
3. Mass and the moment of inertia axis about the three axes.

Using secondary standards traceable to the National Institute for Standards and Technology (NIST), the factory calibration constants (volts per g) of the linear accelerometers were verified in a precision measurement laboratory at the AEDC. The three linear accelerometers comprising a tri-axial group were attached to a cubic block so that the active axes of the accelerometers were orthogonal. Each of the blocks was, in turn, mounted to a plate driven by a linear shaker motor and oscillated to peak levels of 5, 10, 20, 50, and 90 g to check linearity. In all instances, the PMEL calibrations were within 3 percent of the factory calibrations. The linear response that was demonstrated was important in developing the data reduction equations.

Data from the accelerometers that were not in line with the intended axis of oscillation were also recorded to assess unintentional interactions. Interactions on the order of 2 to 3 percent were measured; however, the interactions were dependent on the frequency of oscillation, and were neither in phase nor 180-deg out of phase with respect to the accelerations along the primary axis of oscillation. Therefore, it was concluded that the incidental off-axis motion of the mounting plate driven by the shaker motor was the source of the interactions instead of either misalignment of the accelerometers on the block or mechanical interaction of the accelerometer sensor. It was clear that a calibration capability should be developed to provide a pure linear oscillation (or at least a knowledge of the impurity) so that interactions can be unambiguously identified.

After calibration, the tri-axial accelerometer blocks were mounted in the instrumentation chassis of the KTM at a roll angle of approximately 45 deg as shown in Fig. 12. The instrumentation chassis was then inserted into a model shell. A sensitivity matrix was required to transfer the acceleration data from the block and accelerometer coordinate system to the body axis system of the model. The matrix, which included the effects of rotation of the accelerometers relative to the body axes and the conversion of g's to volts for each accelerometer-amplifier combination, was determined by exciting the completed model with a shaker motor. Fixtures called "calibration bodies" were specifically designed to provide a means of attaching the models to the shaker motor, so that the X, Y, and Z body axes of the model were aligned, in turn, with the oscillation axis of the shaker motor. The model orientation to determine the transformation to the Y axis is illustrated in Fig. 13.

Acceleration data must also be transferred to the center of gravity of the model for use in the trajectory program. The location of each accelerometer relative to the center of gravity of the model

was determined by spinning the models about the X, Y, and Z model body axes on the AEDC Magnus spin rig, using the aforementioned calibration bodies as mounting fixtures. Spinning about the X axis is illustrated in Fig. 14. The models were spun about the body axis system, assuming that the origin of the axis system was located at the model center of gravity. Credibility of the resulting distances was evaluated by comparison with physical measurements of the distances.

Moments of inertia of the models about the body axes were determined using an AEDC inertia meter, which is essentially a torsion spring pendulum. Using the known torsion spring constant, the moment of inertia was determined by measuring the period of a forced rotational oscillation. Models were attached to the inertia meter with the same calibration bodies used with the shaker motor and spin rig. An illustration of the model mounted on the inertia meter to measure the inertia about the Z axis is displayed in Fig. 15.

6.0 TRIAL DROP RESULTS

It is not within the scope of this document to present a quantitative analysis of acceleration, force and moment, or trajectory data recorded using the KTM, but to illustrate functionality of the KTM. Consequently, it is appropriate to compare separation trajectories deduced from conventional film records and from the KTM. Accordingly, trajectories based on film and KTM records for a 1/15-scale model of an aircraft fuel tank released at one condition in Tunnel 4T are illustrated in Fig. 16.

The mass and cg properties of the fuel tank model corresponded to a tank containing only 2 percent of a full load of fuel. Safe separation of such a buoyant body is commonly assured by imposing a delayed release from the aft suspension hook. The delay is accomplished by requiring a pitch-down rotation of the body before disengagement of the aft hook from the body can occur. In flight, the body pitches down severely after release of the forward hook, then tumbles after final release from the aft hook. The intent is to prevent a steady lifting force that would fly the body into contact with the aircraft. Consequently, the trajectory illustrated in Fig. 16, which represents the motion of the cg and attitude of the body axes of the tank relative to the aircraft pylon, is characterized by a strong pitch down with little yaw and roll until separation from the aft hook. Although there are discrepancies in amplitudes, the trends of the independent data sets match reasonably well. Detailed analysis of the data is still underway, but a possible explanation is the difficulty of determining "time zero," i.e., the time of actual disengagement from the aft hook. As an illustration, consider the acceleration data in the Z-axis direction taken during calibration of the spring that simulated the ejector push-off force (Fig. 16). The trace represents the acceleration values in the Z-axis direction in the time domain (accelerometers were sampled 10,000 times each sec, but only every thousandth point is illustrated). Landmark times are indicated with notes. Oscillations prior to release reflect motion of the joined parent and store models. The large, off-

scale excursion of the graph corresponds to the passage of a strong current through the small "burn bolt" that represents the forward hook attachment to the store. The current is strong enough to melt the bolt, causing it to sever, simulating release of the store from the forward hook. It is clearly difficult to identify the exact point in time at which to declare separation of the store model from the forward hook. Consequently, it is difficult to determine when to begin integration of the data points to determine velocity and displacement of the store model. The slope of the curve of the acceleration signal as a function of time is very steep in the vicinity of the burn-bolt spike, and a small change in time (corresponding to a change in selecting time = zero for integration purposes) is accompanied by a large change in acceleration.

Immediately after the burn bolt severs, the spring simulating the ejector force pushes the store model away from the aircraft, and the store model, still restrained by the aft hook, begins to pitch nose-down. As shown in Fig. 17, the accelerometers in the thin-walled plastic store model respond in a dynamic mode during the pitching motion, probably in response to the impulse imparted by the spring. Subsequently, disengagement from the aft hook occurs, the store model enters into free-flight motion, and the data become more coherent. It is important to note that a more complete trajectory can be extracted from telemetry data than from film records, since the store model quickly leaves the field of view of the cameras, while the KTM continues to transmit until impact with the model-catch screen (Fig. 9) or some other obstacle.

Battery life, which is approximately 20 sec, is not an issue, since a trajectory to impact is less than 1 sec, and power to the KTM is not turned on until perhaps 5 sec before the burn-bolt current is activated. Battery performance does provide one concern, however, in the power-discharge characteristics. Although the circuits are assembled of conventional solid-state devices which are imputed to respond instantaneously to applied voltage, full stabilization of voltages at various circuit components does not actually occur until a few seconds have passed (less than five). The challenge, then, is to turn on the KTM soon enough before store model release to provide for voltage stabilization, yet not so far in advance that the batteries are drained of energy before the trajectory is complete.

Future development of the KTM will focus on further reductions in the volume and mass of the module to allow use in a larger set of configurations. Smaller circuit boards and components, and smaller accelerometer transducers which use less power represent a primary desire. A different transmitting technique, such as the spread-spectrum technique of sending multiple channels of data on a single broad-band channel, may also lead to size and weight reductions via a reduction in power, hence a reduction in the volume and mass of the battery-based power supply.

7.0 CONCLUSIONS

Accelerations of a small model in free motion in a wind tunnel have been successfully determined at the AEDC through the use of accelerometers and solid-state telemetry. Cooperative efforts of the aircraft System Program Office (SPO), the user of the test facilities (Lockheed Ft. Worth Company), the Directorates of Flight Test and Technology (AEDC/DOFA and AEDC/DOT, respectively), and the Flight Dynamics Contract Operator (Micro Craft Technology), made possible the design, fabrication, calibration, and testing of four accelerometer/telemetry-equipped models in the short time span of 18 months. Specifically, under a technology effort sponsored by the AEDC/DOT, six linear accelerometers and one velocity sensor were combined with analog-to-digital converters and an eight-channel transmitter, all powered by a lithium battery pack, to create a module small enough to fit within a 1/15th-scale model of an aircraft fuel tank. With sponsorship of the aircraft SPO, four of the modules, called the "kinetic telemetry module" (KTM) were assembled, each with the capability of sensing model accelerations (and roll velocity) during a less-than-1-sec free "flight" and transmitting the data to a receiver and decoder outside the tunnel. The decoded digital data were stored on a personal computer equipped with a 32-bit data acquisition card and custom software. Determination of the mass and cg characteristics of the store models was accomplished by the testing company, Lockheed Ft. Worth Company, in the accustomed manner for free-drop store models. Calibration of the accelerometers in the KTM-equipped store models prior to the test was accomplished by Micro Craft Technology at the AEDC by recording the accelerometer outputs resulting from vibrating and spinning the models about the body axes of the models. A set of matrix equations was developed by Micro Craft Technology (with the sponsorship of AEDC/DOFA), to combine the calibration data with test data and produce a digital description of the trajectory of the freely moving model in the space-time domain.

Several conclusions can be drawn from the development process and the first tests of the KTM-equipped models:

1. Trajectory parameters can be extracted from accelerometer data with lower uncertainty than extractions based on film records.

2. Accelerometer-based trajectory simulations can be longer (in the time domain) and therefore provide more data than film-based trajectories because telemetry is not limited to the field of view of a camera.

3. Trajectories can be extracted from digital accelerometer data and subjected to analysis in hours, as contrasted with days for filmed trajectories.

4. Synchronization of release events is important, since the prime data acquisition window opens a few seconds after the battery-powered KTM circuit is turned on. Data must be acquired after circuit stabilization and before battery power dissipation.

5. Defining time zero, i.e., the time at which release ends and motion begins, is difficult but crucial, since displacements are deduced from mathematical integration (determining the area under the curve) of the acceleration-time relationship, a relationship that is characterized by strong gradients in the region of most difficult definition.

6. The goal of future development of the KTM is to make further reductions in volume occupied by the module by using smaller circuit boards and components, using smaller accelerometer transducers which use less power, and implementing a different transmitting technique, such as the spread-spectrum technique of sending multiple channels of data on a single broad-band channel. All of these changes will allow a reduction in power, which in turn will allow a reduction in the volume and mass of the battery-based power supply. In addition to physical size reduction, improved synchronization of data acquisition with the "burn bolt" initiation of the free-motion trajectory will be implemented.

REFERENCES

1. Carman, J. B., Jr., Hill, D. W., Jr., and Christopher, J. P. "Store Separation Testing Techniques at the Arnold Engineering Development Center, Vol. II, Description of Captive Trajectory Store Separation Testing in the Aerodynamic Wind Tunnel (4T)." AEDC-TR-79-1 (AD-A087561), June 1980.

2. Carman, J. B., Jr. "Store Separation Testing Techniques at the Arnold Engineering Development Center, Vol. I, An Overview."AEDC-TR-79-1, (AD-A087561), June 1980.

3. Allee, E. G., Jr. "Store Separation Testing Techniques at the Arnold Engineering Development Center, Vol. IV, Description of Dynamic Drop Store Separation Testing." AEDC-TR-79-1, (AD-A087561), June 1980.

4. Marquart, E. J. "Development of a Kinematic Telemetry Test Technique for Ground Test Applications in the AEDC Wind Tunnels, Space Chambers, and Gun Ranges." AIAA-94-2579, 18th AIAA Aerospace Ground Testing Conference, Colorado Springs, CO, June 20–23, 1994.

5. Shafer, W. M. "Interim Report — Task 10 Drop Model Telemetry (CDRL 0003)." Lockheed Fort Worth Company Report No. FZM-8333, September 1994.

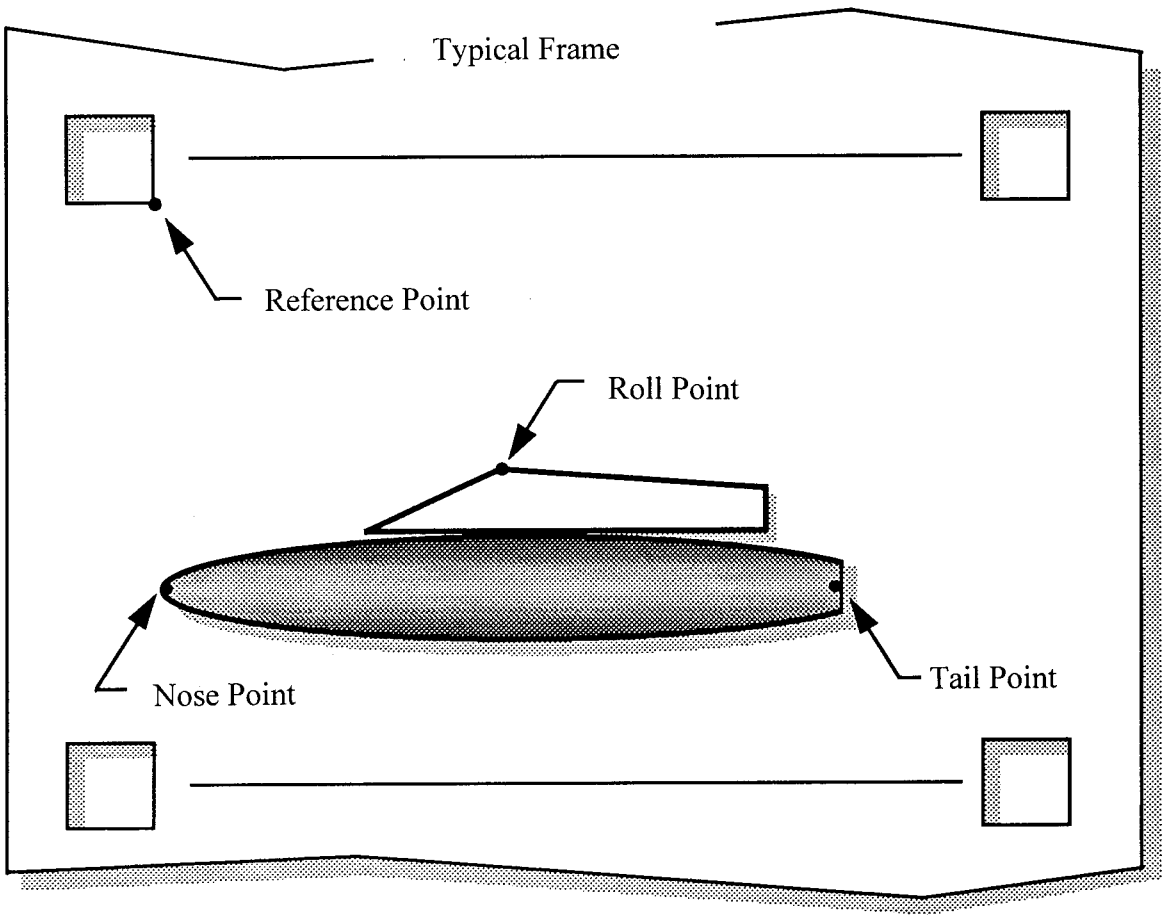

Relative displacements of three points on the model with respect to the reference point are measured in each frame Absolute displacements are determined from knowledge of the size and location of a reference grid on a board mounted in the test section and filmed before the test.

Figure 1. Illustration of the technique of free-drop film analysis.

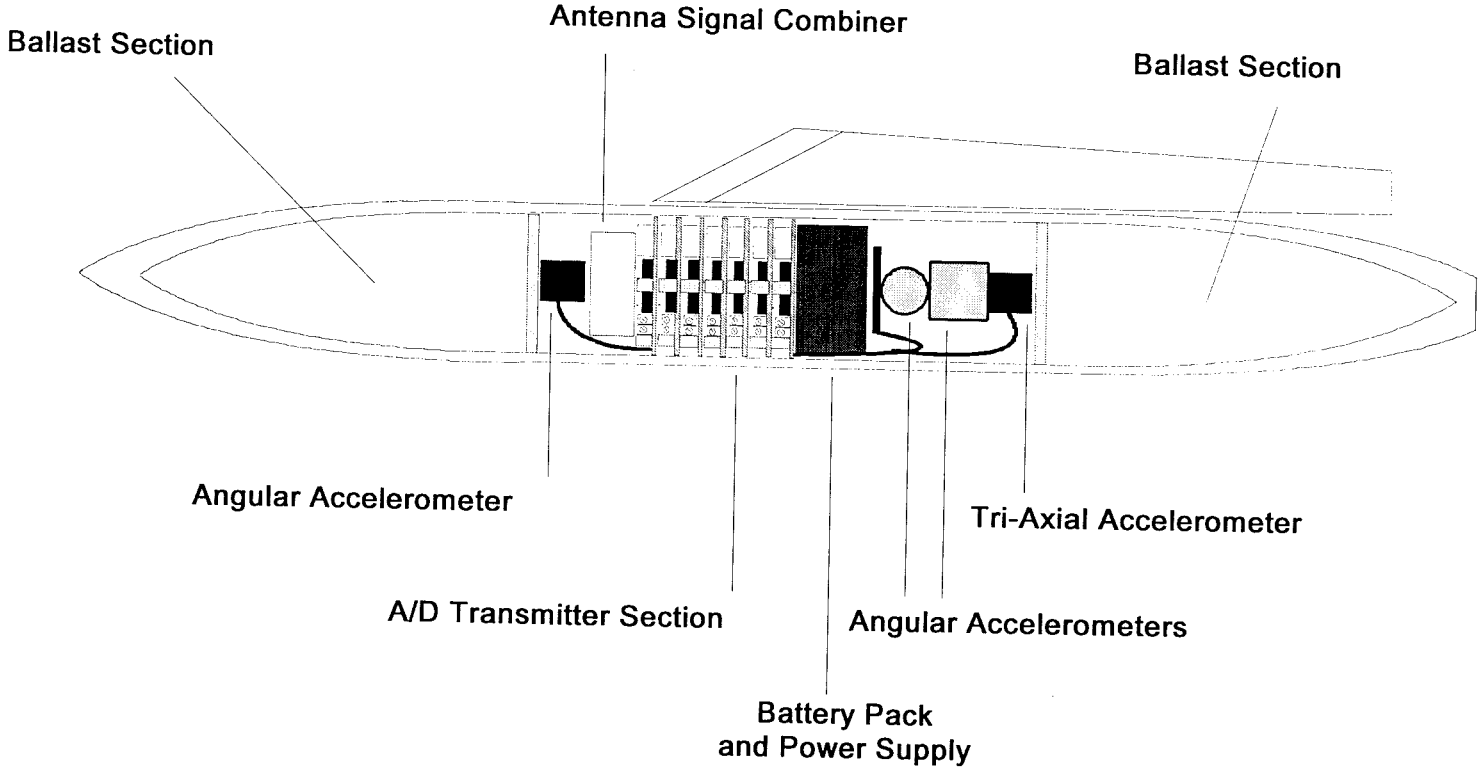

a. Acceleration technique

Figure 2. Conceptual arrangement of components in a free-drop model equipped for acceleration/telemetry tests.

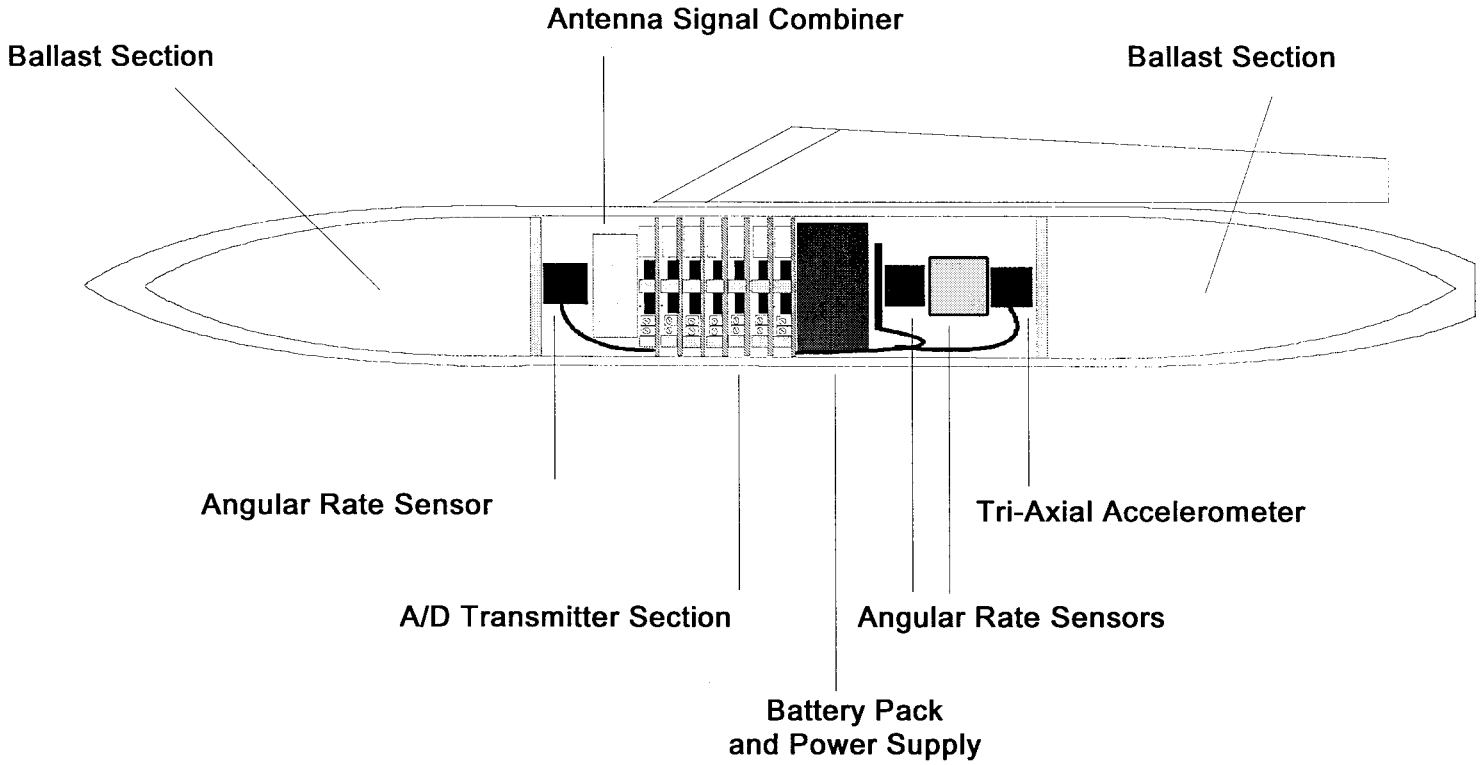

b. Acceleration/rate technique
Figure 2. Continued.

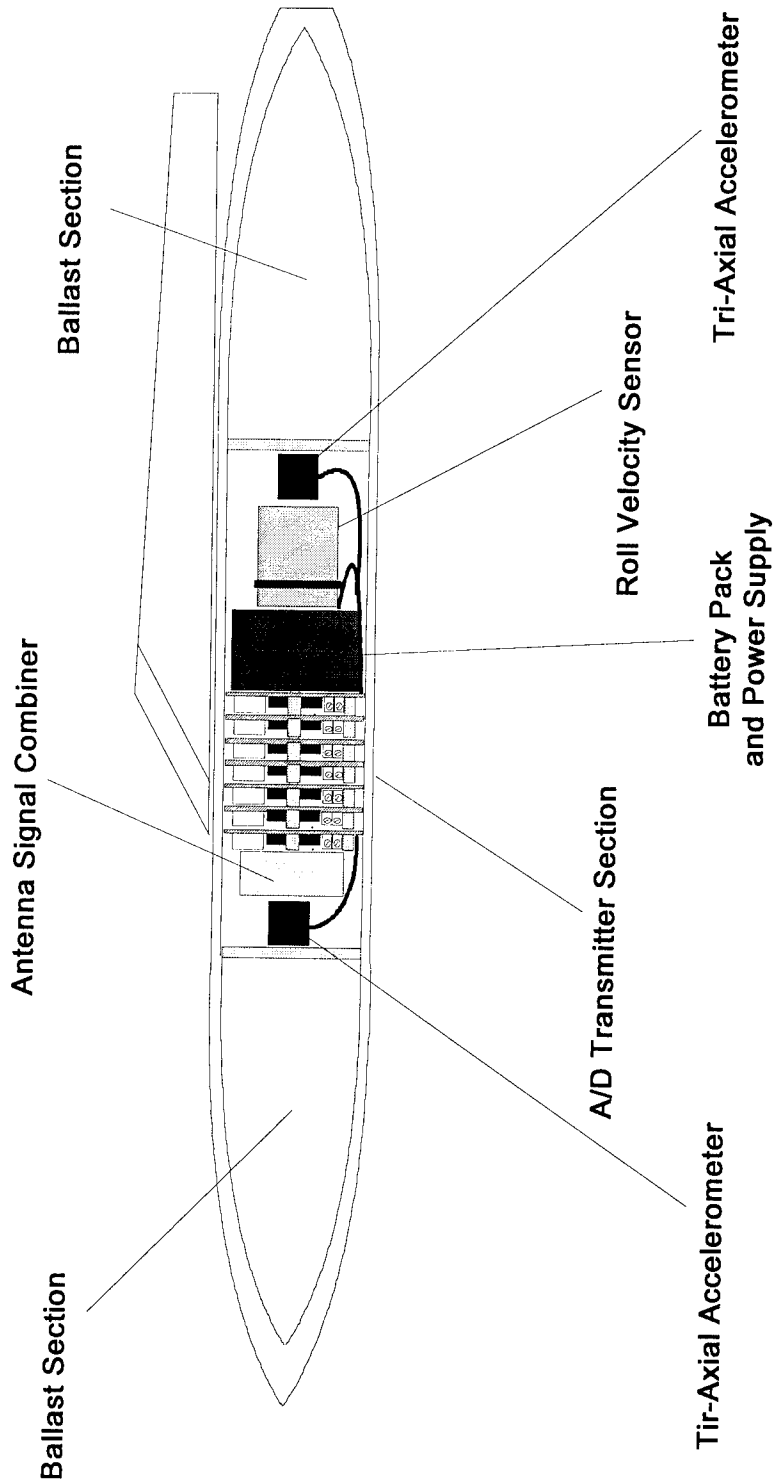

c. Linear/linear technique
Figure 2. Concluded.

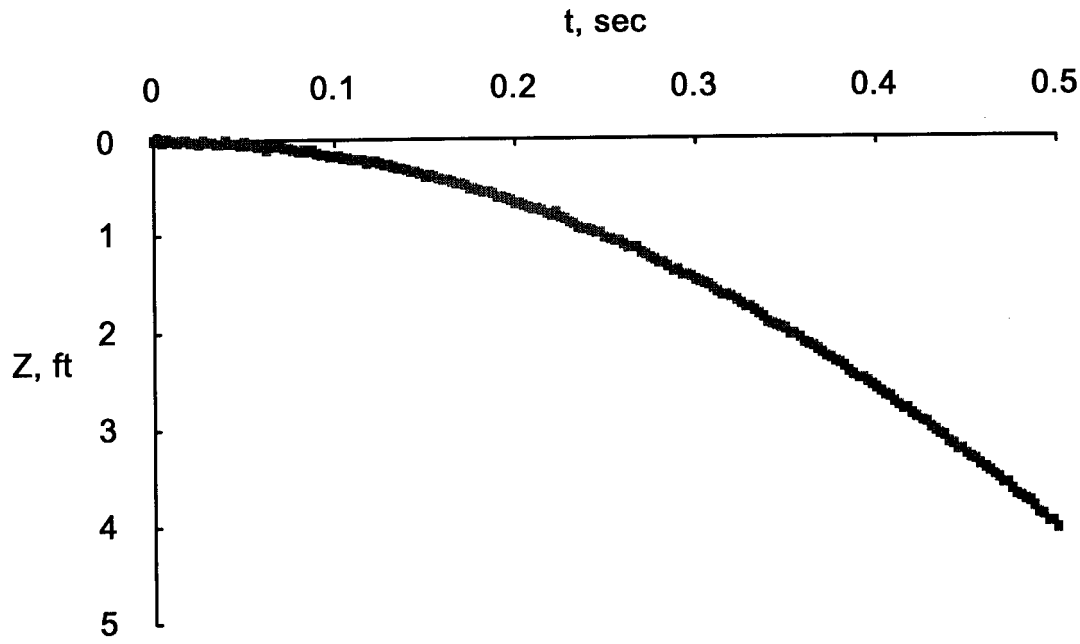

a. Displacement in the vertical, or Z direction

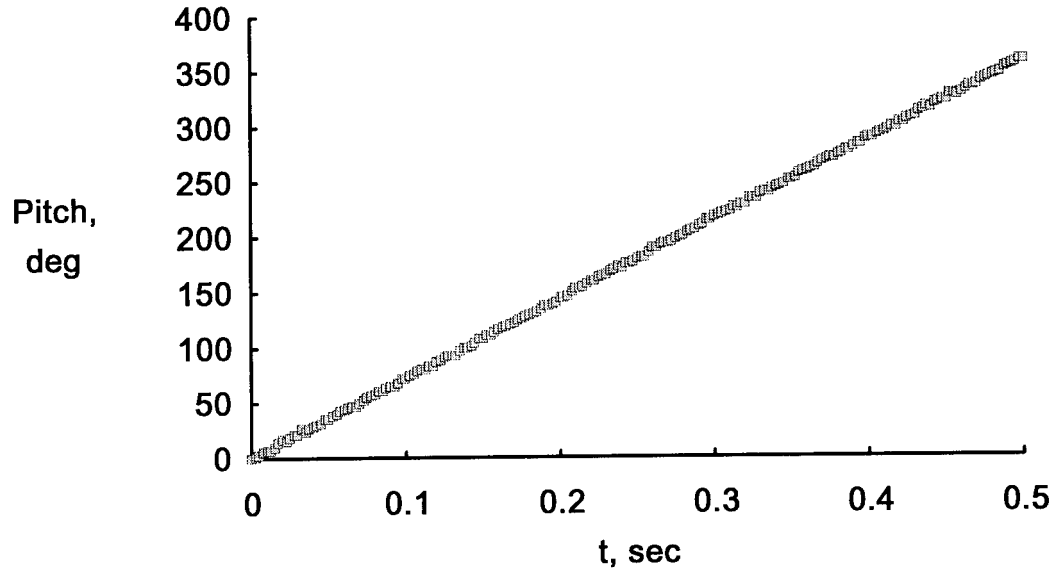

b. Angular displacement in the pitch plane

Figure 3. Hypothetical trajectory of a body in a vacuum, but with photographic method uncertainties superimposed on the calculated values.

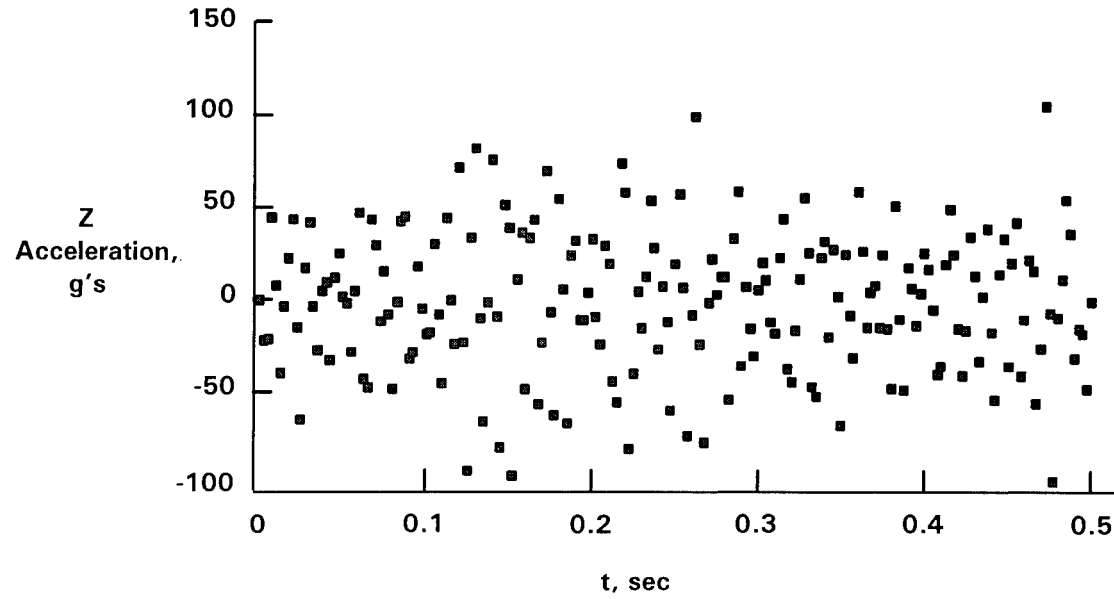

a. Linear acceleration values–Z direction

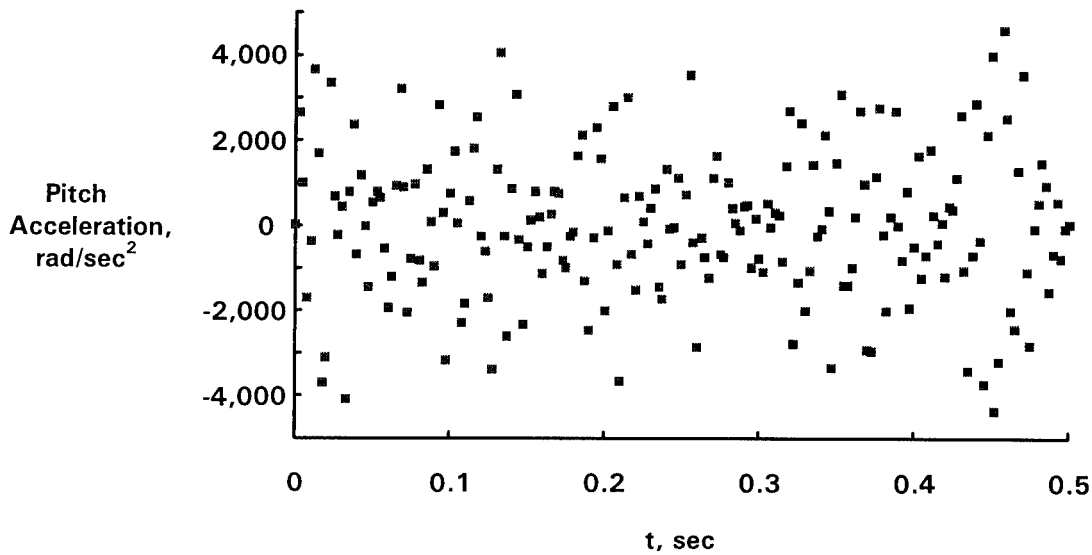

b. Angular accleration values–pitch

Figure 4. Variation in accelerations calculated from a hypothetical trajectory with quoted uncertainties for photographic data reduction superimposed.

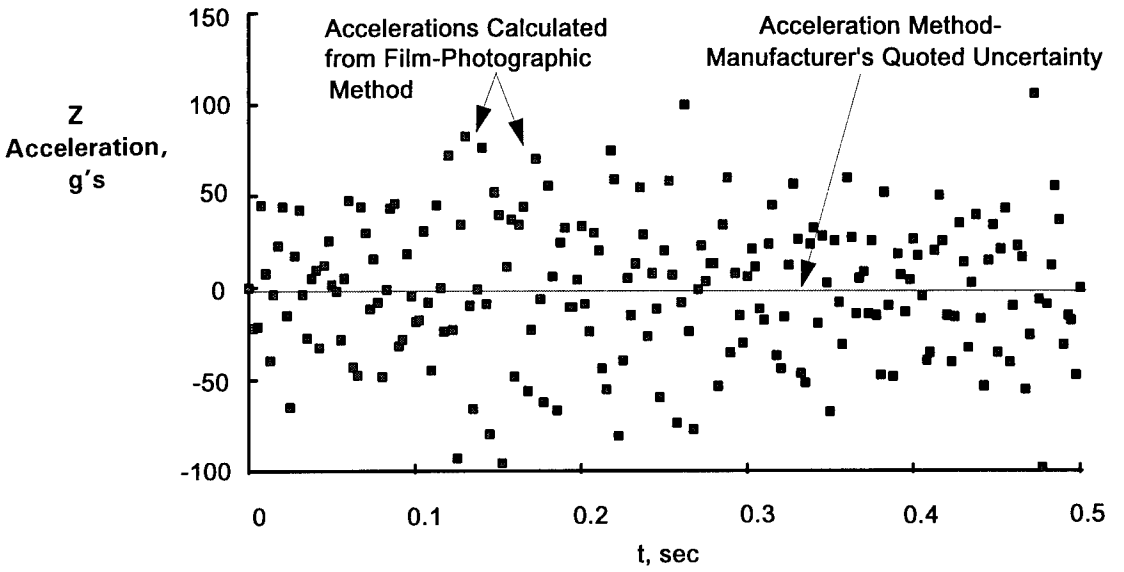

a. Linear acceleration, Z direction

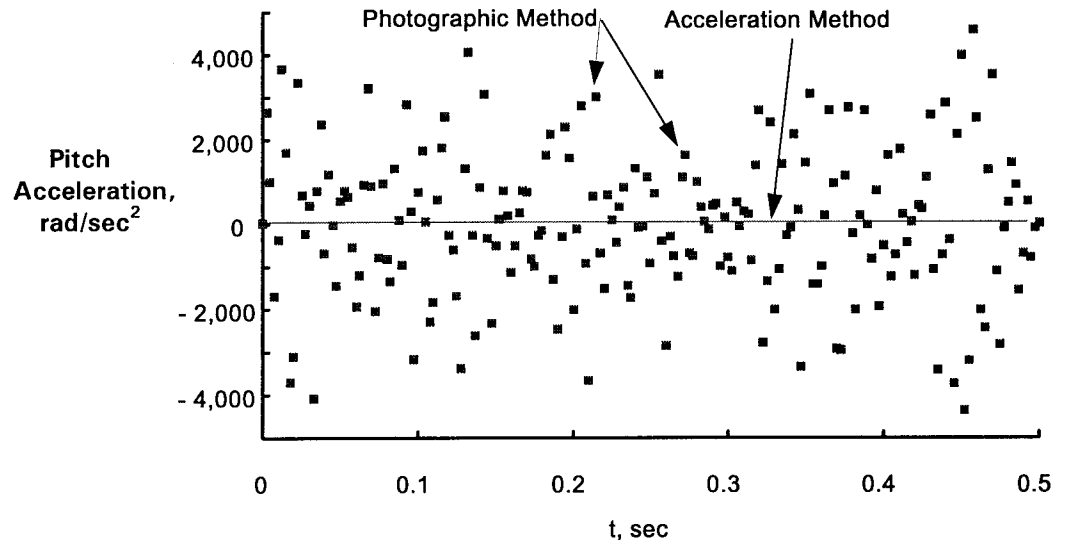

b. Angular acceleration, pitch degree of freedom

Figure 5. Comparison of acceleration method and photographic method accelerations, using quoted uncertainties for each method.

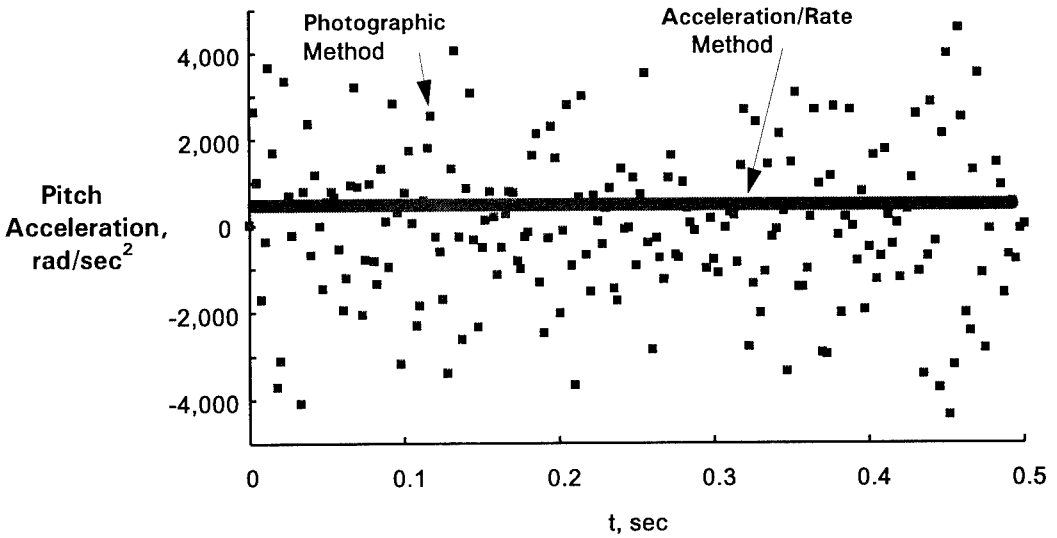

a. Photographic and acceleration/rate techniques compared

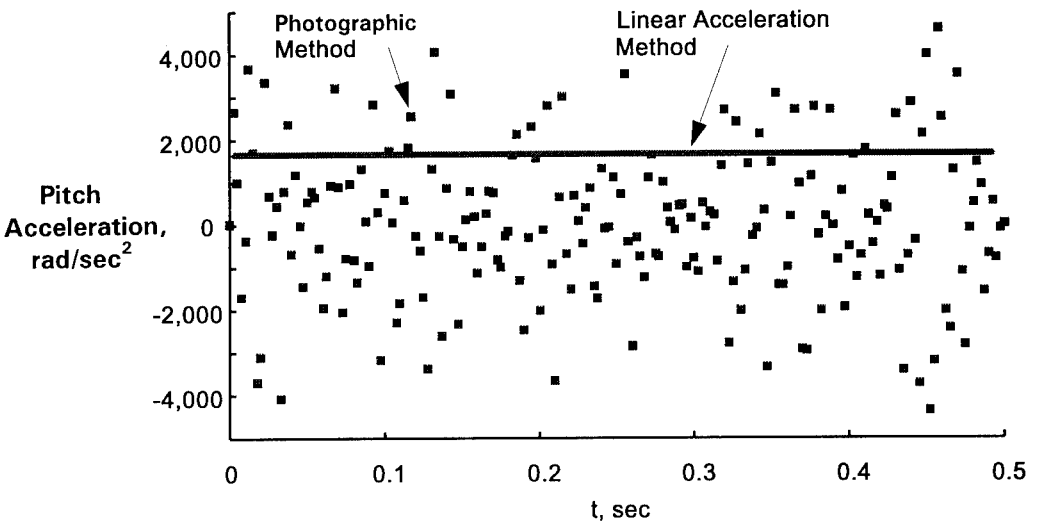

b. Photographic and linear acceleration techniques compared

Figure 6. Comparison of photographic method with accleration/rate and linear acceleration techniques, using quoted uncertainties for each.

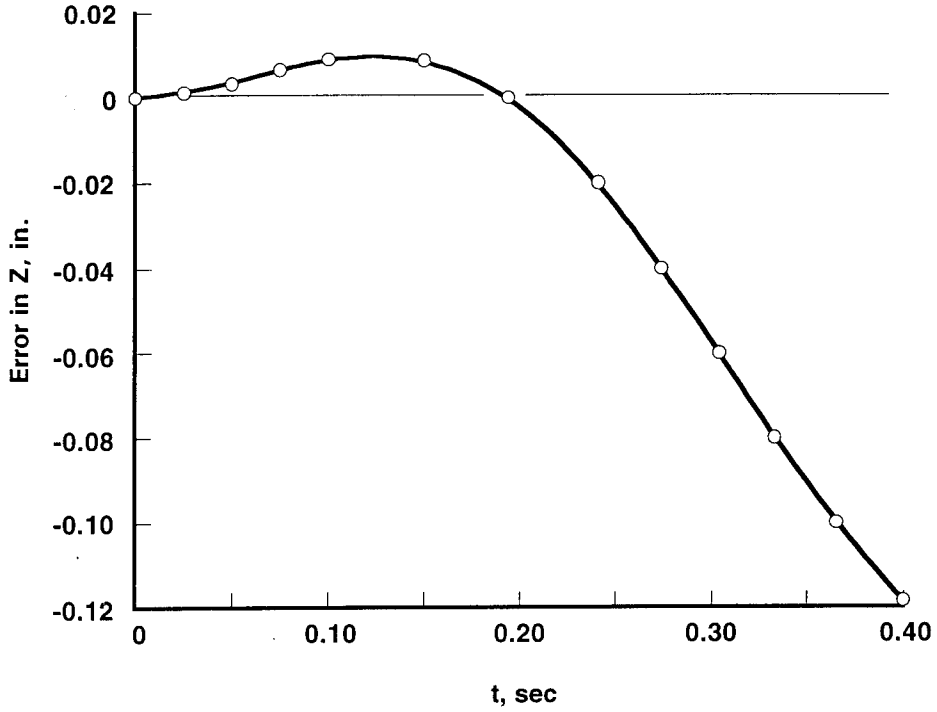

a. Vertical displacement error

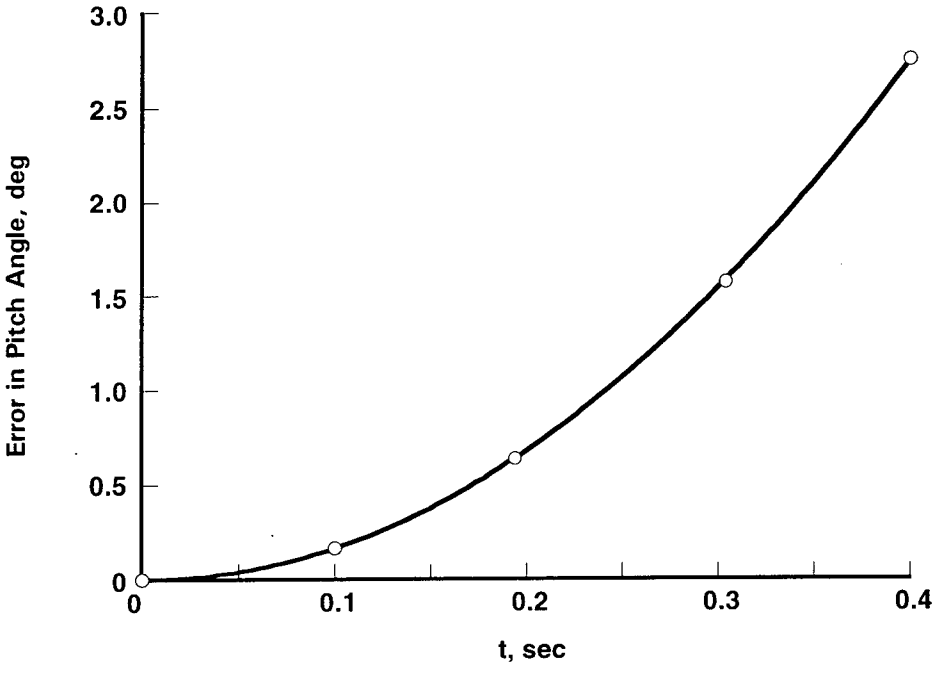

b. Pitch angle error

Figure 7. Variation of errors in accelerometer trajectory parameters with elapsed time during the hypothetical trajectory.

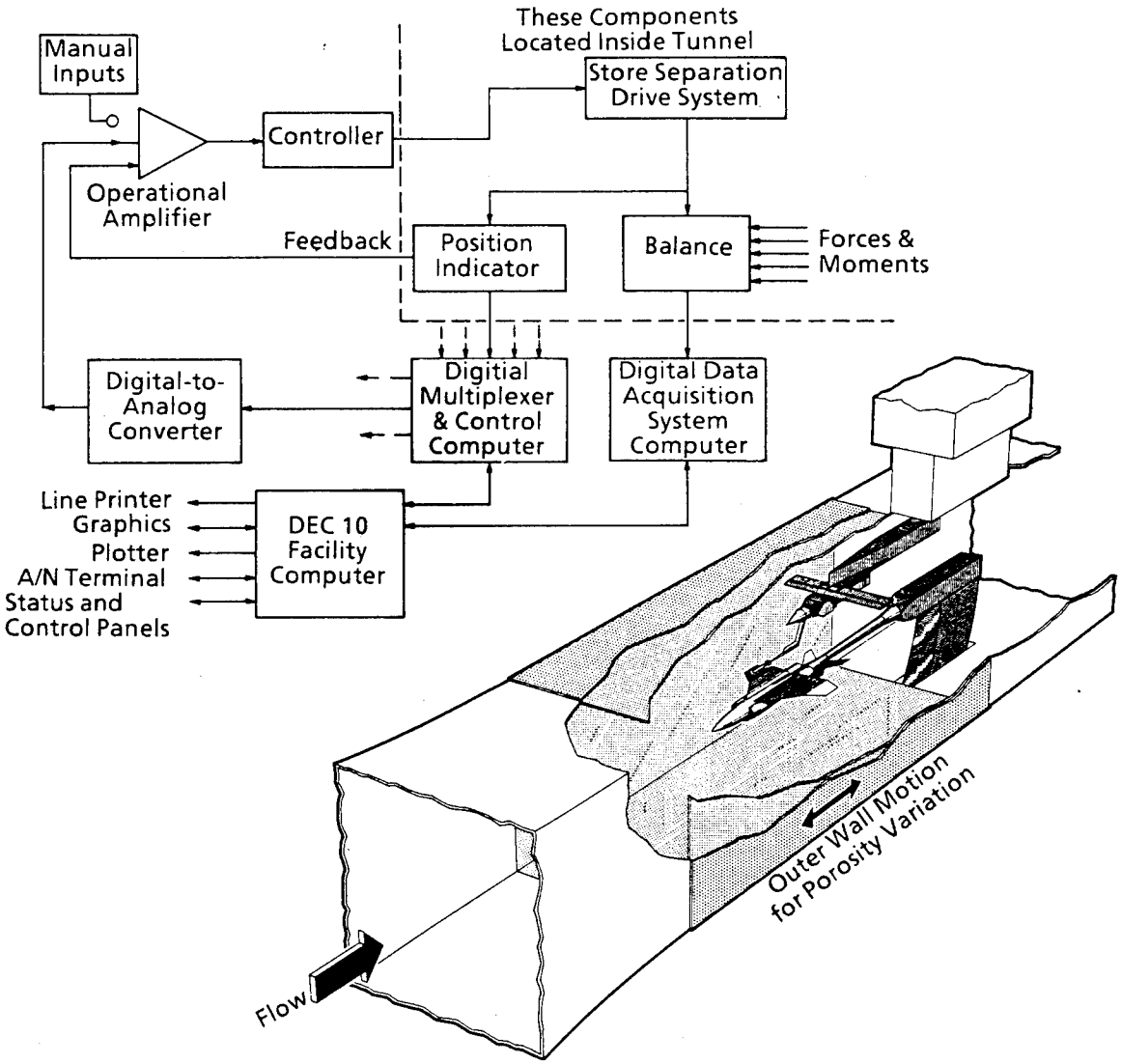

Figure 8. Sketch of the Aerodynamic Wind Tunnel 4T.

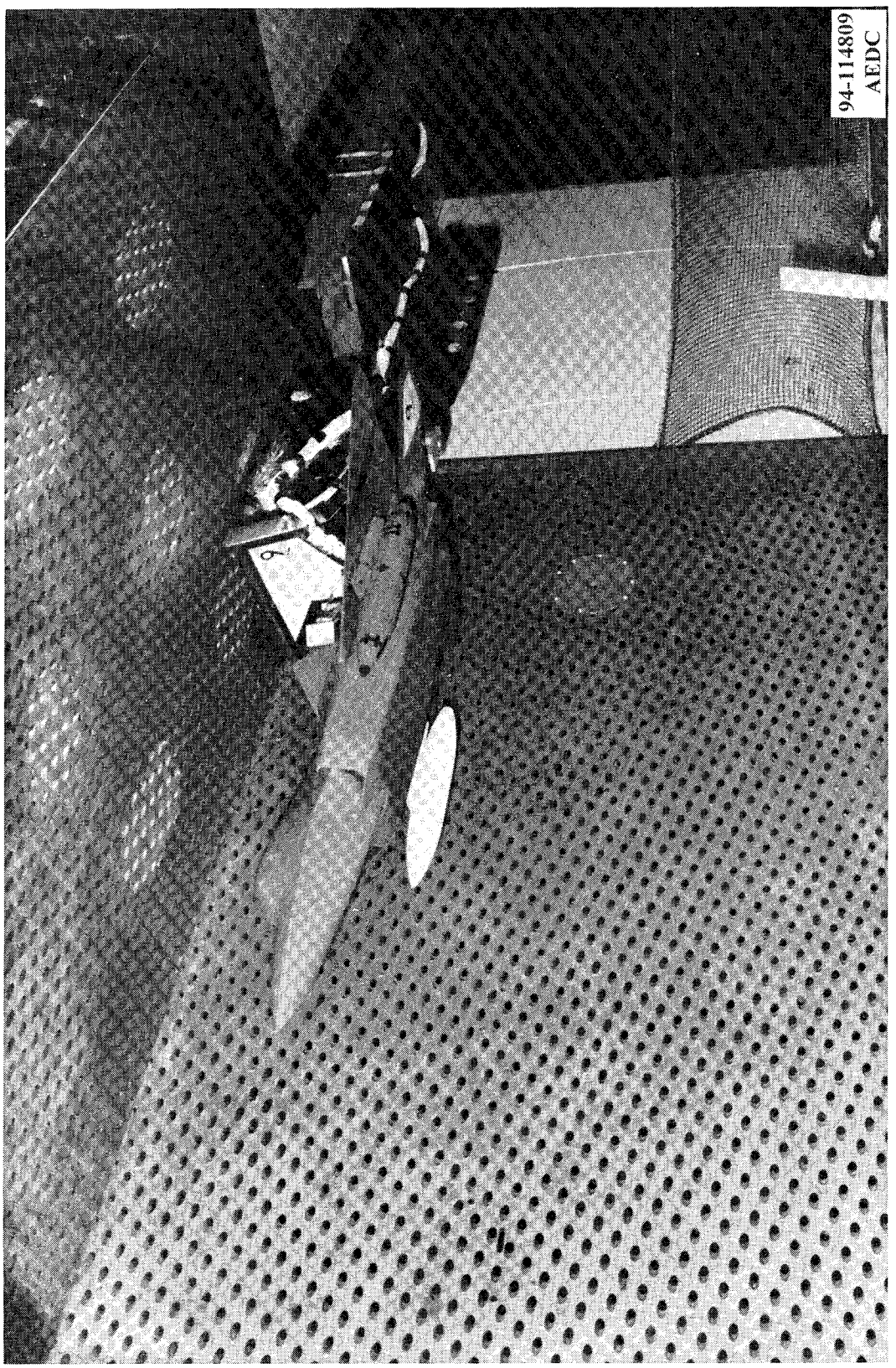

Figure 9. Photograph of a free-drop test installation in Tunnel 4T.

Dimensions and Stations in Inches

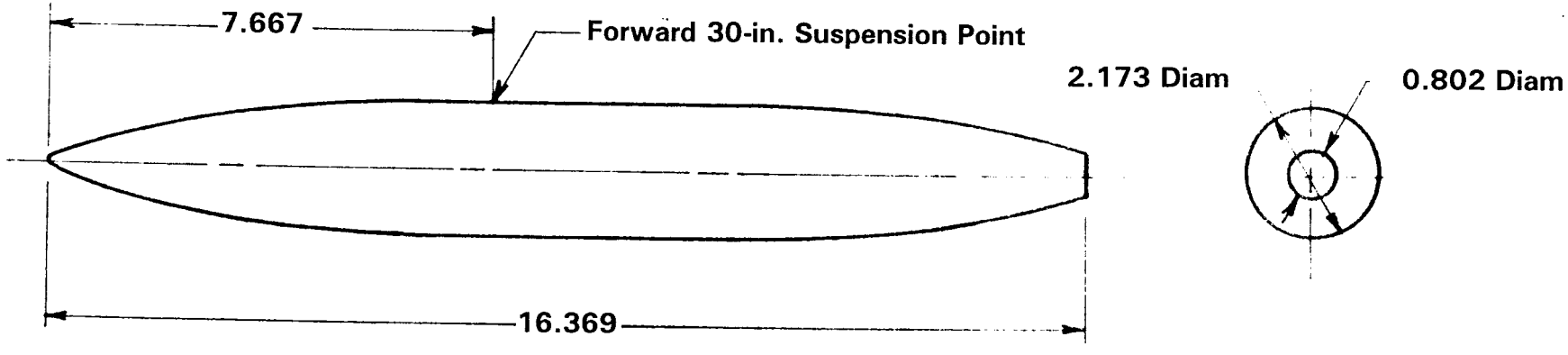

Figure 10. Dimensions of the fuel tank model.

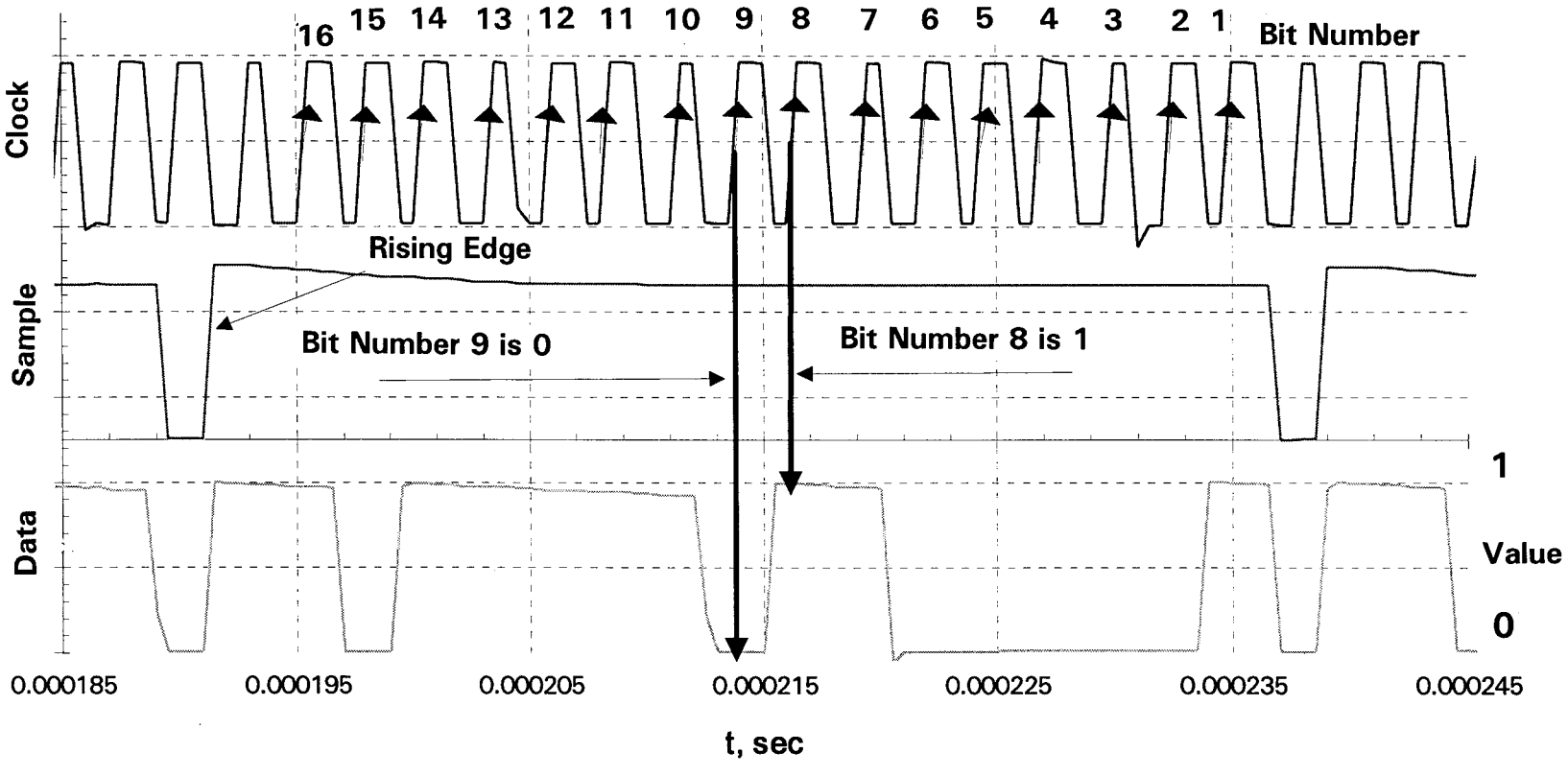

Figure 11. Recovery of data from a modulated signal.

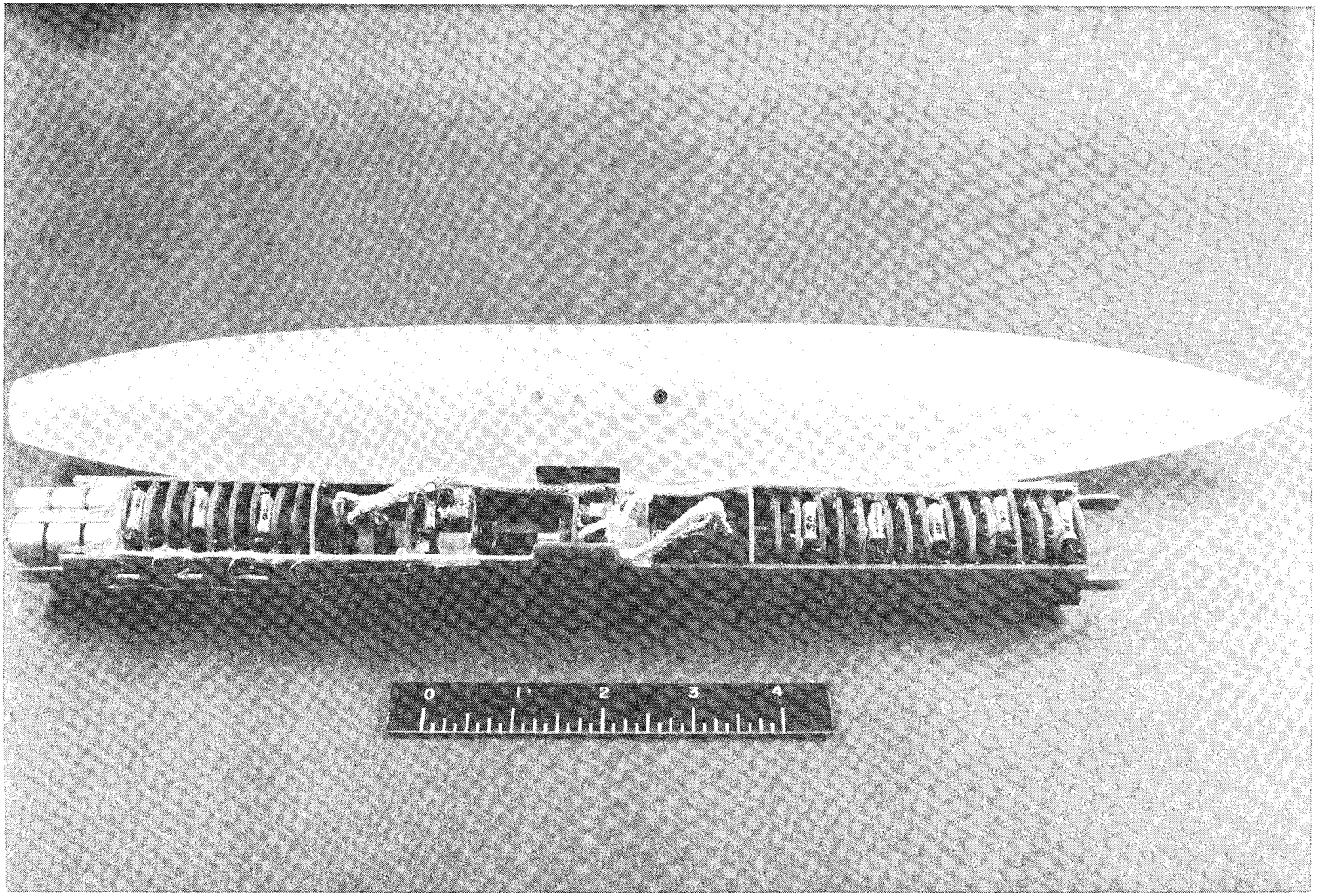

Figure 12. Photograph of the KTM and the fuel tank model.

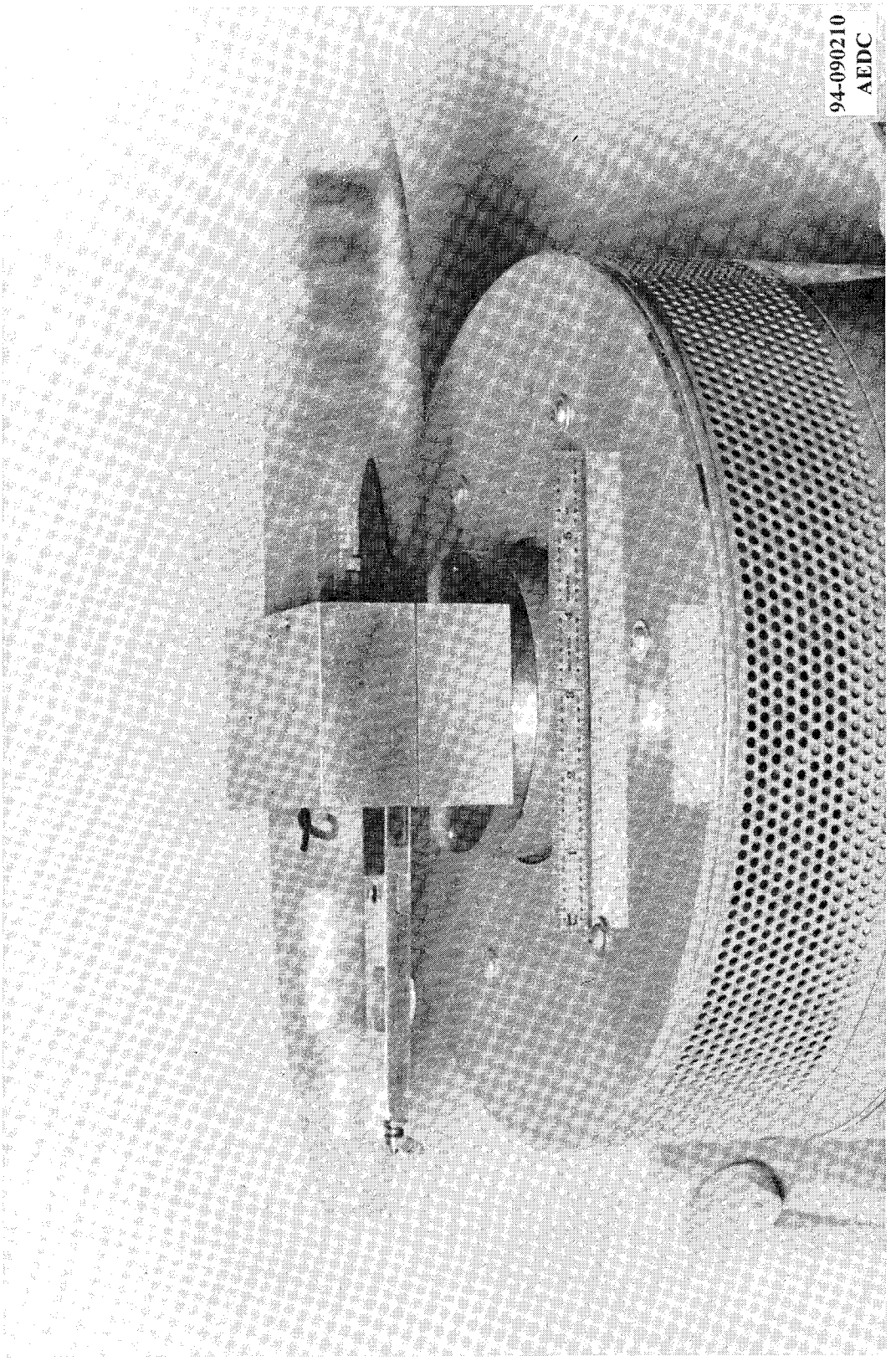

Figure 13. Photograph of the complete model mounted on a shaker for Y-axis calibration.

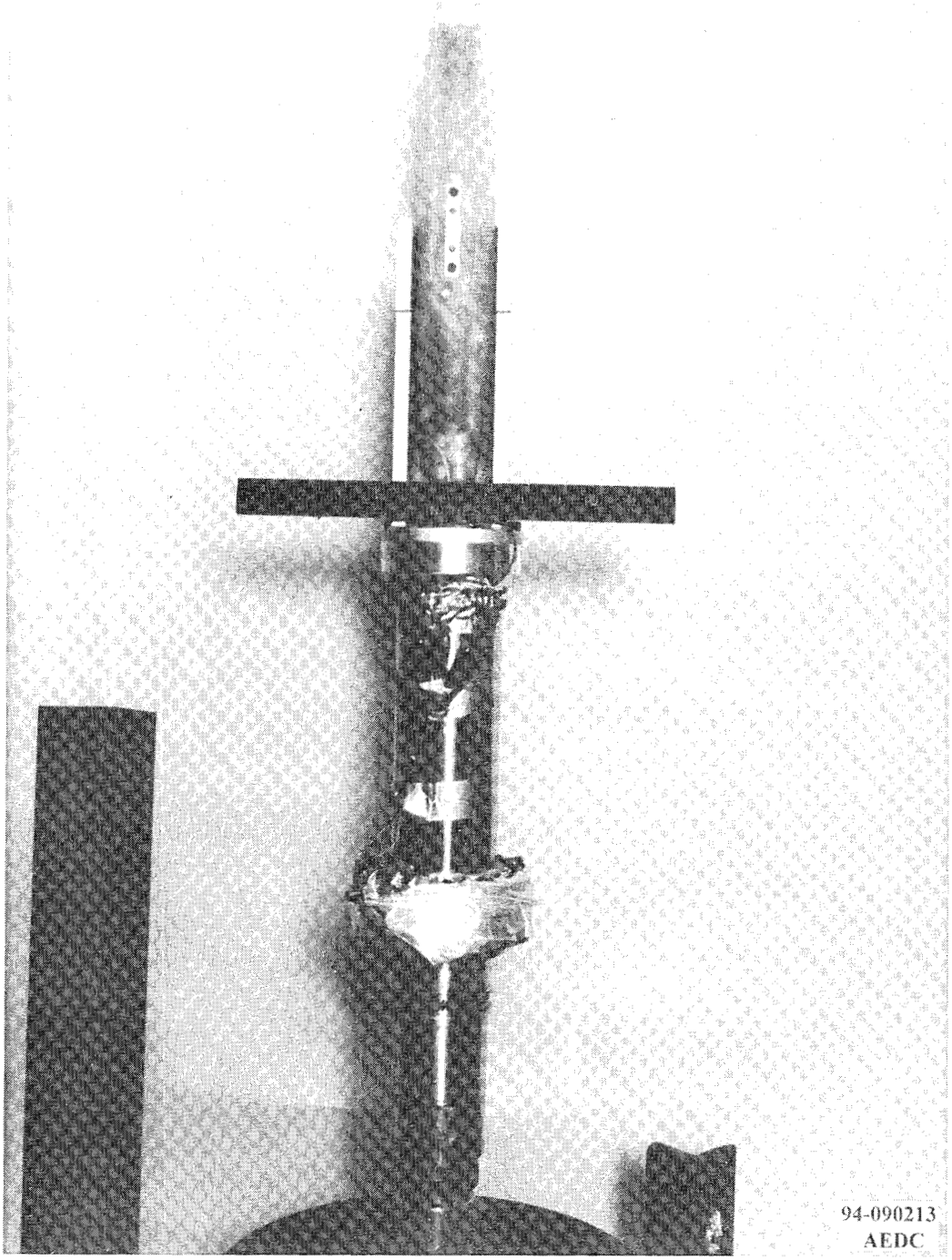

Figure 14. Photograph of the complete model mounted on a spin rig for a roll calibration.

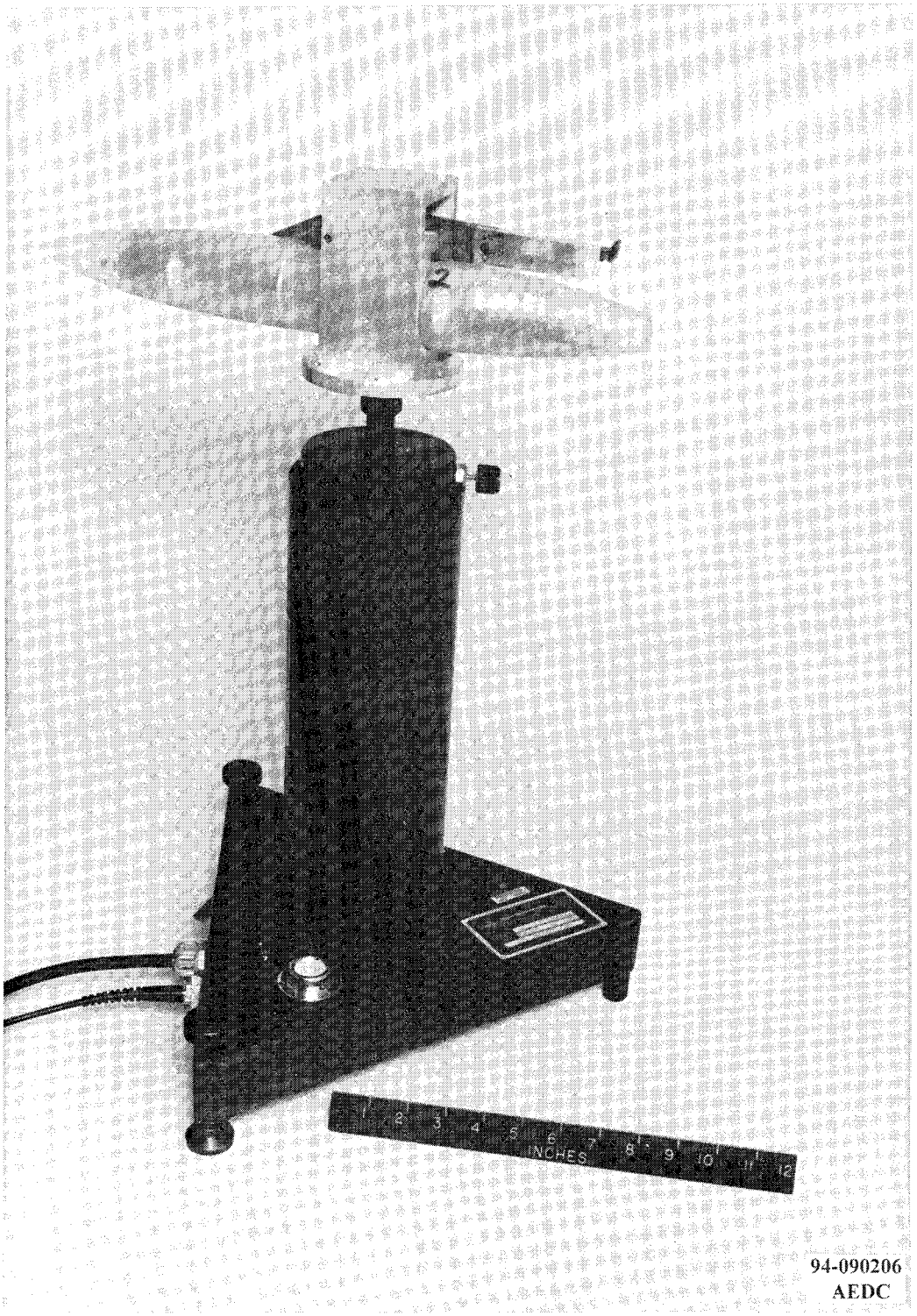

Figure 15. Photograph of the complete model mounted on an inertia meter for Z-axis calibration.

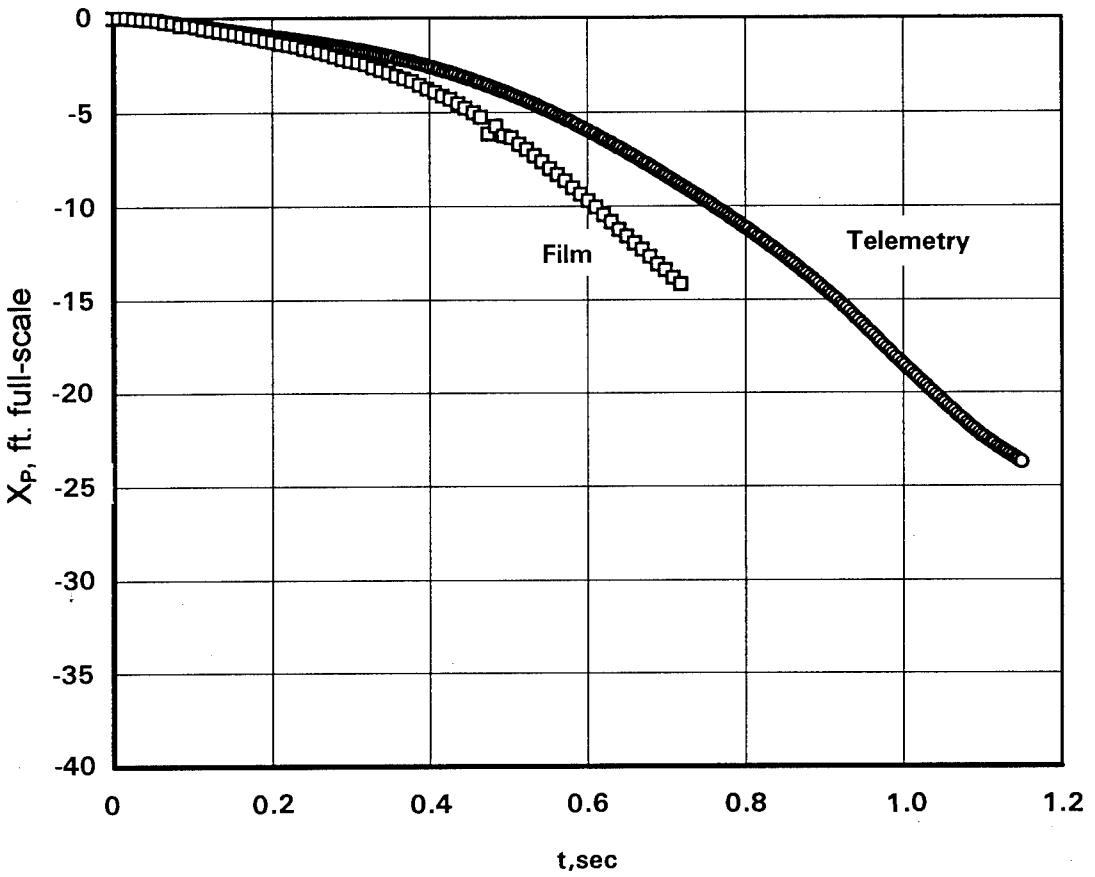

a. Longitudinal displacement

Figure 16. Comparison of film-based and telemetry-based fuel tank trajectories.

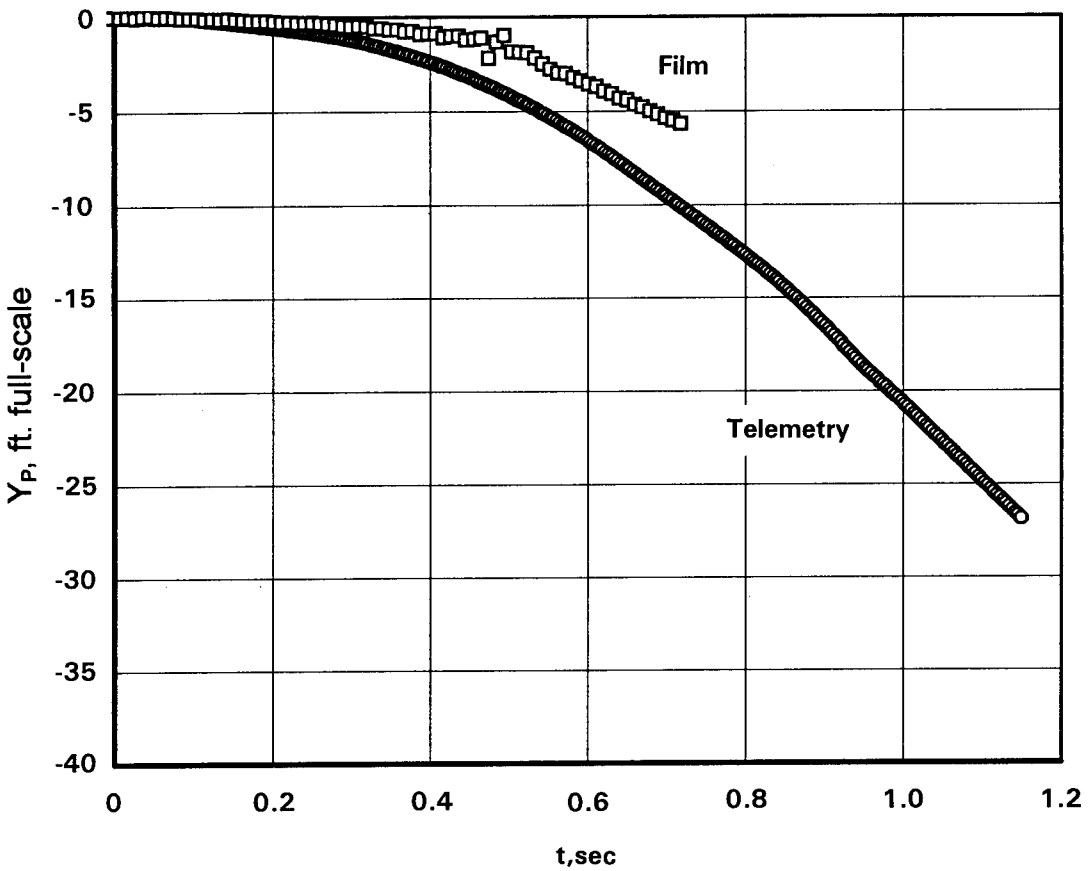

b. Lateral displacement

Figure 16. Continued.

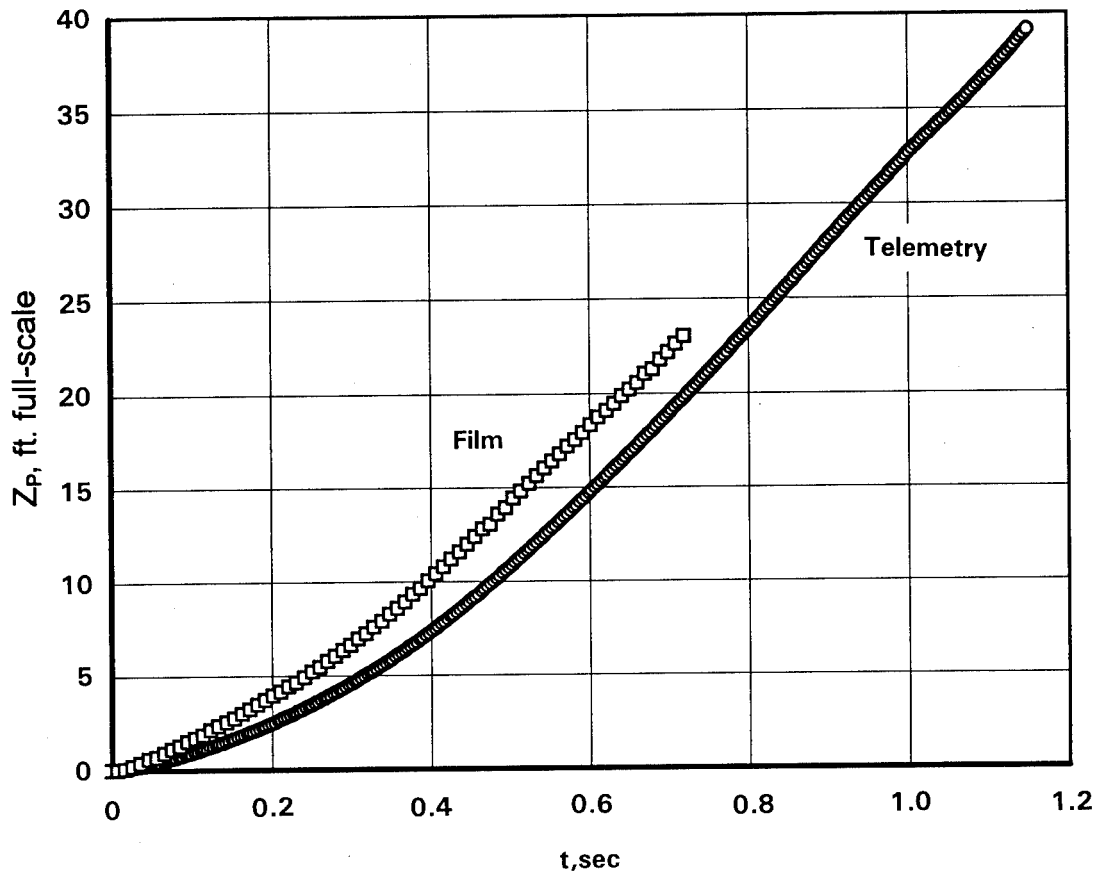

c. Vertical displacement

Figure 16. Continued.

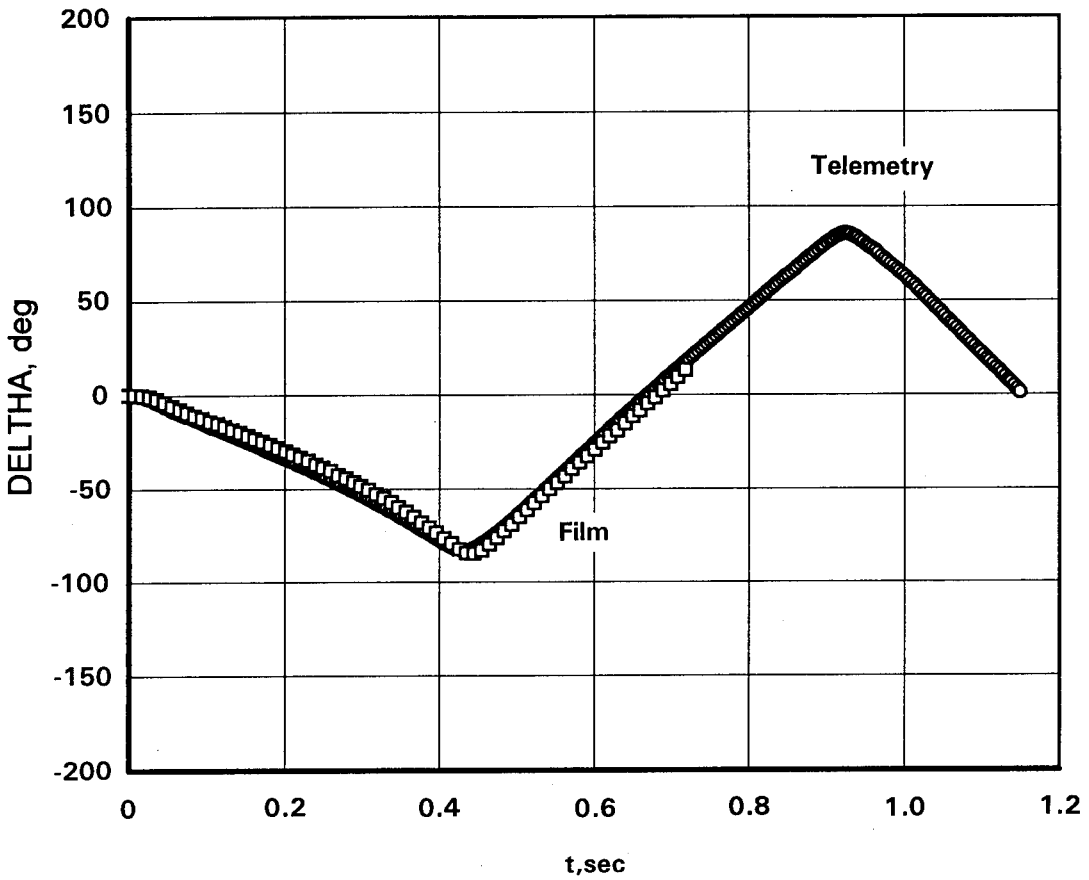

NOTE: Angular displacements beyond ±90 deg in pitch appear to decrease because of rigid quadrant-selection rules in the data reduction equations. Actual pitch displacement extends continuously toward a complete revolution of the store.

d. Pitch displacement
Figure 16. Continued.

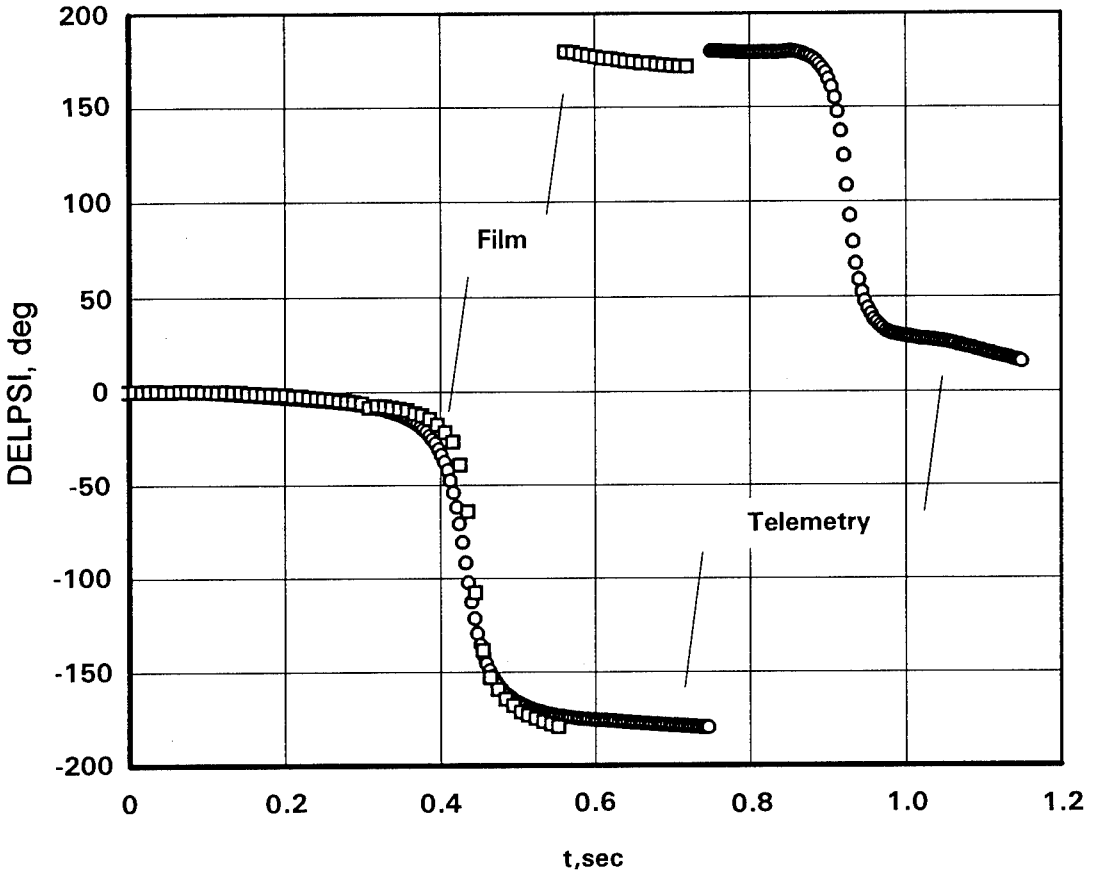

NOTE: Angular displacement beyond ±180 deg of yaw appears to be discontinuous because of rigid quadrant-selection rules in the data reduction equations. Actual yaw displacement extends continuously toward a complete revolution of the store.

e. Yaw displacement
Figure 16. Continued.

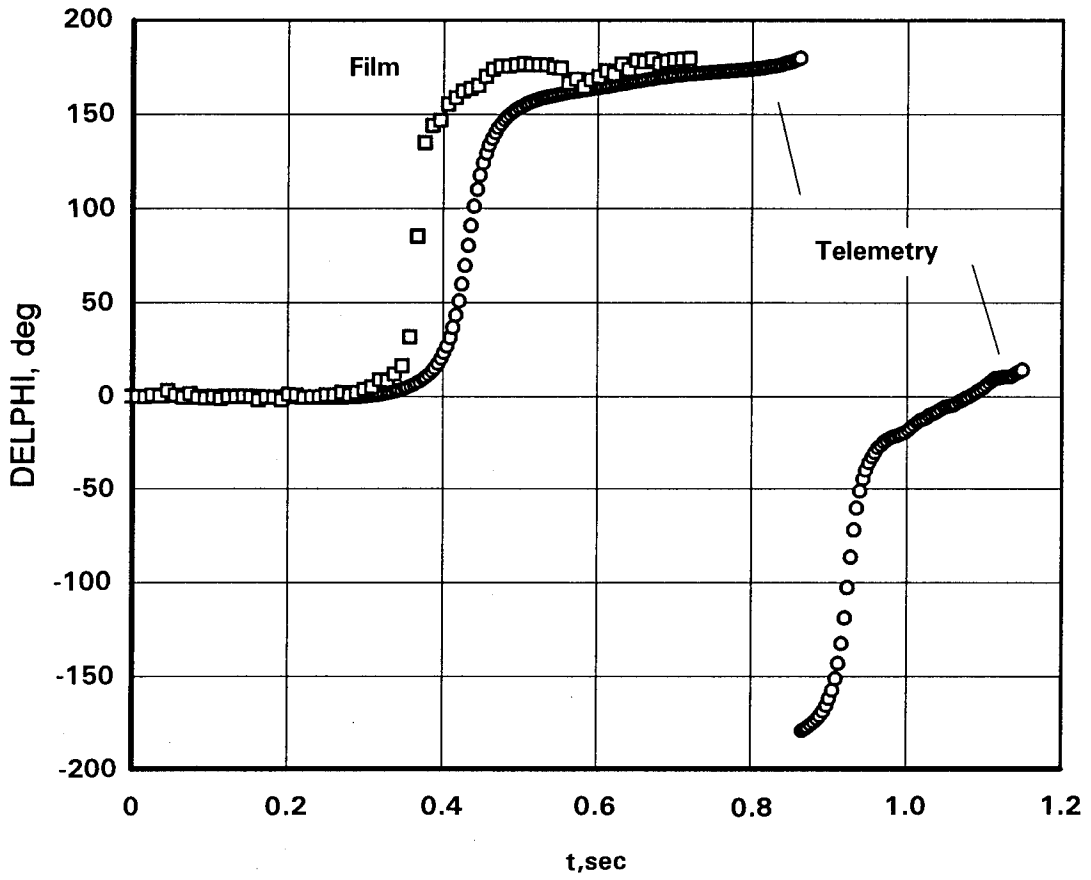

NOTE: Angular displacement beyond ±180 deg of roll appears to be discontinuous because of rigid quadrant-selection rules in the data reduction equations. Actual roll displacement extends continuously toward a complete revolution of the store.

f. Roll displacement

Figure 16. Concluded.

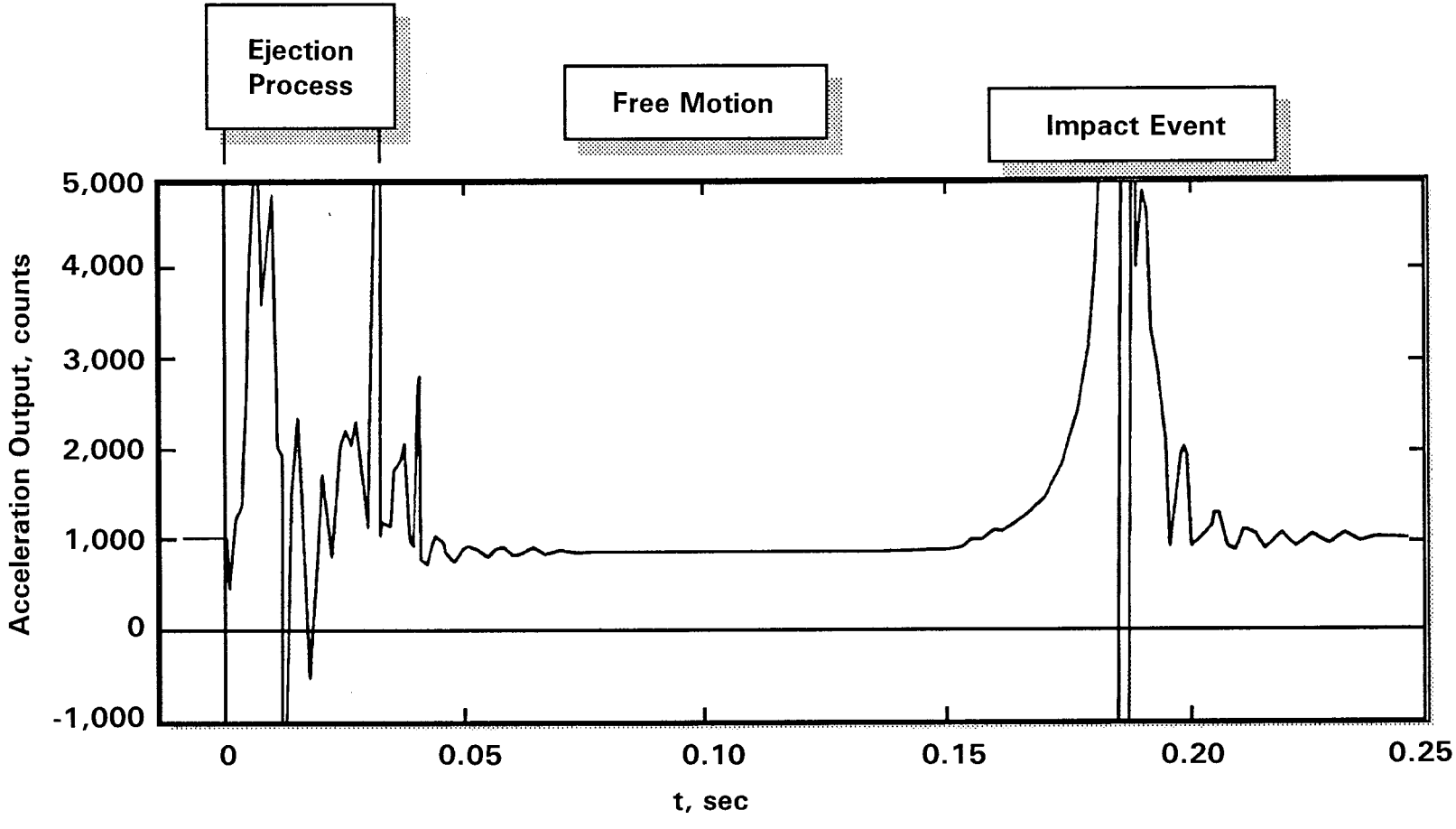

Figure 17. Accelerometer output in the Z-axis direction during ejector spring calibration.

APPENDIX A
CALIBRATION EQUATIONS

It was assumed, to preserve generality, that the installed orientation of each transducer in the model (the roll-velocity sensor and each of the six linear accelerometers) was unique. By design, each accelerometer was sensitive to accelerations in just one direction, but the challenge was to determine that direction relative to the body axes of the model after the KTM was installed. Although both the forward (nose) and aft (tail) arrays of linear accelerometers consisted of three separate transducers mounted on three adjacent faces of cubical mounting blocks, it was not assumed that the resulting tri-axial arrays were either orthogonal, or characterized by a common point of measurement corresponding to the intersection of the three axes of sensitivity. Consequently, a set of matrix equations involving a separate translation matrix for each accelerometer was written to translate the component accelerations in the accelerometer axis system to the body axis system at the cg of the model.

Nomenclature for the equations needed to reduce the accelerometer data to a usable format is complicated, at best, and deserves separate description. All upper-case symbols are used to facilitate comparison of equations with data-reduction codes written in the FORTRAN language. First, accelerometer output is a voltage, which is referred to in conventional instrumentation parlance as "counts." Parameters representing values in counts of acceleration along some direction X are designated as "CAX." The sensed accelerations including the presence of gravity — are indicated by an "M" for "measured." After the "M," the selected accelerometer is specified, using as a designation the block on which it is mounted (an "N" for an accelerometer mounted on the block in the forebody region of the model, or a "T" for an accelerometer mounted on the block in the afterbody region of the model) with a subscript indicating the Cartesian X, Y, or Z direction of the axis of maximum sensitivity of the accelerometer. Next, the direction of interest in the axis system of the block is indicated by an "N" or "T" with a Cartesian X, Y, or Z subscript. Finally, the inertial axis system is clearly in use, and is indicated by an "I." As an example, the quantity $CAXMN_XN_XI$ designates the component of the "counts of acceleration in some X direction, sensed by the X-direction accelerometer attached to the forebody block, acting in the X-direction of the forebody block, with respect to the inertial axis system." Similarly, the quantity $GAXMN_XN_XI$ denotes the number of g's of acceleration at the forebody block, instead of counts.

When the model is mounted in a laboratory setting in an upright attitude as illustrated, (i.e., as if attached for straight-and-level flight), the accelerations that would be sensed by accelerometers aligned with the body axes are

$$\begin{Bmatrix} GAXMBBI \\ GAYMBBI \\ GAZMBBI \end{Bmatrix} = \begin{Bmatrix} 0 \\ 0 \\ -1 \end{Bmatrix} g\text{'s} \qquad \text{(A-1)}$$

where the negative sign indicates the reaction required to hold the model in place.

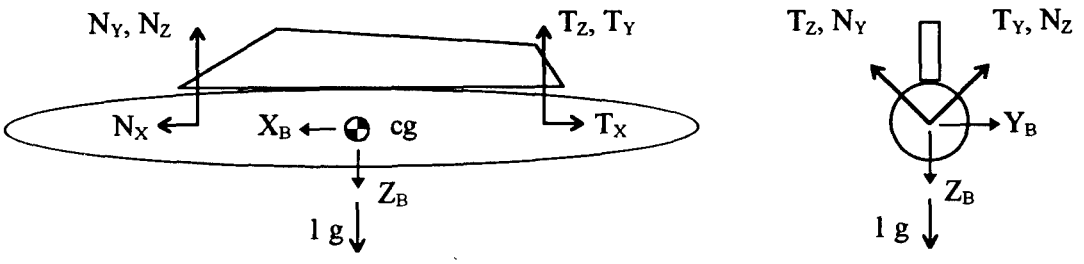

Similarly, when the model is mounted on its side in the lab, as illustrated, the accelerations that

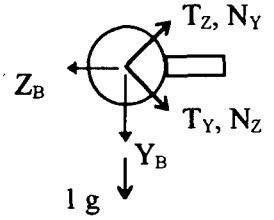

Looking Forward

would be sensed by accelerometers aligned with the body axes can be represented by Eq. (A-2).

$$\begin{Bmatrix} GAXMBBI \\ GAYMBBI \\ GAZMBBI \end{Bmatrix} = \begin{Bmatrix} 0 \\ -1 \\ 0 \end{Bmatrix} g\text{'s} \tag{A-2}$$

Further, when the model is mounted on end (vertically) in the lab, as illustrated, the accelerations that would be sensed by accelerometers aligned with the body axes can be represented by

$$\begin{Bmatrix} GAXMBBI \\ GAYMBBI \\ GAZMBBI \end{Bmatrix} = \begin{Bmatrix} 1 \\ 0 \\ 0 \end{Bmatrix} g\text{'s} \tag{A-3}$$

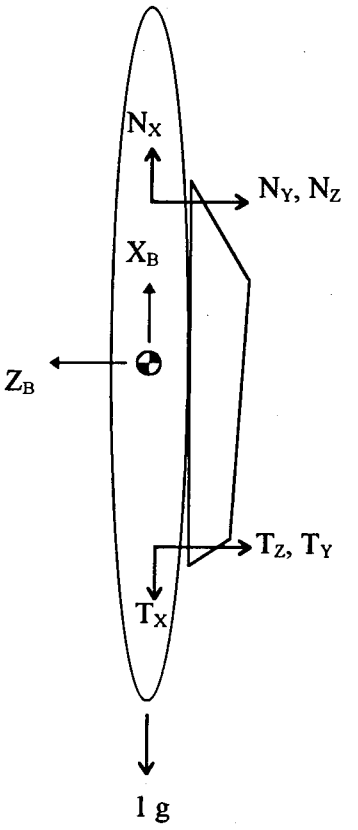

In all cases, the accelerations actually sensed by the installed accelerometers comprise a set of electrical output signals in counts (millivolts), represented by

$$\begin{Bmatrix} CAXMN_XN_XI \\ CAYMN_YN_YI \\ CAZMN_ZN_ZI \end{Bmatrix} \tag{A-4}$$

A conversion from counts to g's requires a transformation matrix involving the sensitivity of the accelerometers in g's per count, represented by Eq. (A-5)

$$\begin{Bmatrix} GAXMBN_XI \\ GAYMBN_YI \\ GAZMBN_ZI \end{Bmatrix} = [CTRNNB]^{-1} = \begin{Bmatrix} CAXMN_XN_XI \\ CAYMN_YN_YI \\ CAZMN_ZN_ZI \end{Bmatrix} \tag{A-5}$$

where the matrix $[CTRNNB]^{-1}$ includes both the calibration from counts to g's and the $[TRNN_iB]$ matrix for the rotation of the accelerometer data into the body axis coordinate system.

Since the triple accelerometer arrays are comprised of three linear accelerometers mounted on adjacent faces of a cubical block, each accelerometer sensing acceleration in only one direction, no measured accelerations exist in directions that are not aligned with the accelerometers. Hence, for the nose array,

$$\begin{Bmatrix} CAXXNI \\ CAYXNI \\ CAZXNI \end{Bmatrix} = \begin{Bmatrix} CAMXNI \\ 0 \\ 0 \end{Bmatrix} \tag{A-6}$$

$$\begin{Bmatrix} CAXYNI \\ CAYYNI \\ CAZYNI \end{Bmatrix} = \begin{Bmatrix} CAMYNI \\ 0 \\ 0 \end{Bmatrix} \tag{A-7}$$

$$\begin{Bmatrix} CAXZNI \\ CAYZNI \\ CAZZNI \end{Bmatrix} = \begin{Bmatrix} 0 \\ 0 \\ CAMZNI \end{Bmatrix} \tag{A-8}$$

where the quantities in the left-hand members of the equations represent the measured outputs of the accelerometers. Once aligned with the body axes, the accelerometers will only relate the acceleration in the direction aligned with the axis of sensitivity, so that

$$\begin{Bmatrix} GAXMBN_XI \\ GAYMBN_XI \\ GAZMBN_XI \end{Bmatrix} = \begin{Bmatrix} GAXMBBI \\ 0 \\ 0 \end{Bmatrix} \tag{A-9}$$

$$\begin{Bmatrix} GAXMBN_YI \\ GAYMBN_YI \\ GAZMBN_YI \end{Bmatrix} = \begin{Bmatrix} 0 \\ GAYMBBI \\ 0 \end{Bmatrix} \tag{A-10}$$

$$\begin{Bmatrix} GAXMBN_ZI \\ GAYMBN_ZI \\ GAZMBN_ZI \end{Bmatrix} = \begin{Bmatrix} 0 \\ 0 \\ GAZMBBI \end{Bmatrix} \tag{A-11}$$

Equations (A-9) –(A-11) can then be written as

$$\begin{Bmatrix} GAXMBBI \\ 0 \\ 0 \end{Bmatrix} = [CTRNXNB]^{-1} \begin{Bmatrix} CAMXNI \\ 0 \\ 0 \end{Bmatrix} \tag{A-12}$$

$$\begin{Bmatrix} 0 \\ GAYMBBI \\ 0 \end{Bmatrix} = [CTRNYNB]^{-1} \begin{Bmatrix} 0 \\ CAMYNI \\ 0 \end{Bmatrix} \tag{A-13}$$

$$\begin{Bmatrix} 0 \\ 0 \\ GAZMBBI \end{Bmatrix} = [CTRNZNB]^{-1} \begin{Bmatrix} 0 \\ 0 \\ CAMZNI \end{Bmatrix} \tag{A-14}$$

where the quantities *GAiMBBI* ($i = X\ Y$, and Z) are the outputs of the X, Y, and Z accelerometers, respectively, when aligned with the body axes.

The transfer matrices $[TRNN_XB]^{-1}$, etc., may be written in the form

$$[TRNN_xB]^{-1} = \begin{bmatrix} x_{11} & x_{12} & x_{13} \\ x_{21} & x_{22} & x_{23} \\ x_{31} & x_{32} & x_{33} \end{bmatrix} \tag{A-15}$$

so that Eqs. (A-12) – (A-14) become

$$\begin{Bmatrix} GAXMBBI \\ GAYMBBI \\ GAZMBBI \end{Bmatrix} = \begin{bmatrix} x_{11} & x_{12} & x_{31} \\ y_{12} & y_{22} & y_{32} \\ z_{13} & z_{23} & z_{33} \end{bmatrix} \begin{Bmatrix} CAMXNI \\ CAMYNI \\ CAMZNI \end{Bmatrix} \tag{A-16}$$

Now, for a simple 1-g downward acceleration acting on the upright model, the values of the accelerometers in counts sensed by the accelerometers in the body axis can be written as

$$\begin{Bmatrix} CAMXNI \\ CAMYNI \\ CAMZNI \end{Bmatrix} = \begin{Bmatrix} CAXMN_XN_XI \\ CAXYMN_YN_YI \\ CAZMN_ZN_ZI \end{Bmatrix} \tag{A-17}$$

and the vector of acceleration in g's is

$$\begin{Bmatrix} GAXMBBI \\ GAYMBBI \\ GAZMBBI \end{Bmatrix} = \begin{Bmatrix} GAX11 \\ GAY11 \\ GAZ11 \end{Bmatrix} = \begin{Bmatrix} 0 \\ 0 \\ -1 \end{Bmatrix} g\text{'s} \tag{A-18}$$

Similarly, a simple 1-g downward acceleration acting on the model rolled 90-deg right wing down causes values of the accelerometers in counts in the body axis to be

$$\begin{Bmatrix} CAMXNI \\ CAMYNI \\ CAMZNI \end{Bmatrix} = \begin{Bmatrix} CAXMNy\ N_XI \\ CAYMN_yN_yI \\ CAZMN_yN_z \end{Bmatrix} \tag{A-19}$$

and the acceleration vector, in g's to be

$$\begin{Bmatrix} GAXMBBI \\ GAYMBBI \\ GAZMBBI \end{Bmatrix} = \begin{Bmatrix} GAX22 \\ GAY22 \\ GAZ22 \end{Bmatrix} = \begin{Bmatrix} 0 \\ -1 \\ 0 \end{Bmatrix} \text{g's} \tag{A-20}$$

Finally, a simple 1-g downward acceleration acting on the model supported vertically, nose up, causes values of the accelerometers in counts in the body axis to be

$$\begin{Bmatrix} CAMXNI \\ CAMYNI \\ CAMZNI \end{Bmatrix} = \begin{Bmatrix} CAMN_ZN_XI \\ CAYN_ZN_YI \\ CAMN_ZN_ZI \end{Bmatrix} \tag{A-21}$$

and the acceleration vector, in g's to be

$$\begin{Bmatrix} GAXMBBI \\ GAYMBBI \\ GAZMBBI \end{Bmatrix} = \begin{Bmatrix} GAX33 \\ GAY33 \\ GAZ33 \end{Bmatrix} = \begin{Bmatrix} 1 \\ 0 \\ 0 \end{Bmatrix} \text{g's} \tag{A-22}$$

Substituting, the translation matrices, there results

$$\begin{bmatrix} x_{11} & x_{12} & x_{13} & y_{11} & y_{12} & y_{13} & z_{11} & z_{12} & z_{13} \\ x_{21} & x_{22} & x_{23} & y_{21} & y_{22} & y_{23} & z_{21} & z_{22} & z_{23} \\ x_{31} & x_{32} & x_{33} & y_{31} & y_{32} & y_{33} & z_{31} & z_{32} & z_{33} \end{bmatrix} \begin{Bmatrix} CAMXN11 \\ 0 \\ 0 \\ 0 \\ CAMYN11 \\ 0 \\ 0 \\ 0 \\ CAMZN11 \end{Bmatrix} = \begin{Bmatrix} 0 \\ 0 \\ -1 \end{Bmatrix} \tag{A-23}$$

$$\begin{bmatrix} x_{11} & x_{12} & x_{13} & y_{11} & y_{12} & y_{13} & z_{11} & z_{12} & z_{13} \\ x_{21} & x_{22} & x_{23} & y_{21} & y_{22} & y_{23} & z_{21} & z_{22} & z_{23} \\ x_{31} & x_{32} & x_{33} & y_{31} & y_{32} & y_{33} & z_{31} & z_{32} & z_{33} \end{bmatrix} \begin{Bmatrix} CAMXN22 \\ 0 \\ 0 \\ 0 \\ CAMYN22 \\ 0 \\ 0 \\ 0 \\ CAMZN22 \end{Bmatrix} = \begin{Bmatrix} 0 \\ 1 \\ 0 \end{Bmatrix} \tag{A-24}$$

and

$$\begin{bmatrix} x_{11} & x_{12} & x_{13} & y_{11} & y_{12} & y_{13} & z_{11} & z_{12} & z_{13} \\ x_{22} & x_{22} & x_{23} & y_{21} & y_{22} & y_{23} & z_{21} & z_{22} & z_{23} \\ x_{31} & x_{32} & x_{33} & y_{31} & y_{32} & y_{33} & z_{31} & z_{32} & z_{33} \end{bmatrix} \begin{Bmatrix} CAMXN33 \\ 0 \\ 0 \\ 0 \\ CAMYN33 \\ 0 \\ 0 \\ 0 \\ CAMYN33 \end{Bmatrix} = \begin{Bmatrix} 0 \\ 1 \\ 0 \end{Bmatrix} \tag{A-25}$$

Multiplying, the first rows of the results become, for the upright model with 1-g acting down

$$x_{11}CAMXN11 + y_{12}CAMYN11 + z_{13}CAMZN11 = 0 \tag{A-26}$$

$$x_{21}CAMXN11 + y_{22}CAMYN11 + z_{23}CAMZN11 = 0 \tag{A-27}$$

and

$$x_{31}CAMXN11 + y_{32}CAMYN11 + z_{33}CAMZN11 = -1 \tag{A-28}$$

The resulting matrix system is

$$\begin{Bmatrix} GAX11 \\ GAY11 \\ GAZ11 \end{Bmatrix} = \begin{Bmatrix} x_{11}y_{12}z_{13} \\ x_{21}\ y_{22}z_{23} \\ x_{31}y_{32}z_{33} \end{Bmatrix} \begin{Bmatrix} CAMXN11 \\ CAMYN11 \\ CAMZN11 \end{Bmatrix} = \begin{Bmatrix} 0 \\ 0 \\ -1 \end{Bmatrix} \tag{A-29}$$

$$\begin{Bmatrix} GAX22 \\ GAY22 \\ GAZ22 \end{Bmatrix} = \begin{Bmatrix} x_{11}y_{12}z_{13} \\ x_{21}\ y_{22}z_{23} \\ x_{31}y_{32}z_{33} \end{Bmatrix} \begin{Bmatrix} CAMXN22 \\ CAMYN22 \\ CAMZN22 \end{Bmatrix} = \begin{Bmatrix} 0 \\ 0 \\ 1 \end{Bmatrix} \tag{A-30}$$

$$\begin{Bmatrix} GAX33 \\ GAY33 \\ GAZ33 \end{Bmatrix} = \begin{Bmatrix} x_{11}y_{12}z_{13} \\ x_{21}\ y_{22}z_{23} \\ x_{31}y_{32}z_{33} \end{Bmatrix} \begin{Bmatrix} CAMXN33 \\ CAMYN33 \\ CAMZN33 \end{Bmatrix} = \begin{Bmatrix} 0 \\ 0 \\ 1 \end{Bmatrix} \tag{A-31}$$

The calibrated translation matrix can now be written as

$$\left[CTRNNB\right]^{-1} \begin{Bmatrix} x_{11}y_{12}z_{13} \\ x_{21}\ y_{22}z_{23} \\ x_{31}y_{32}z_{33} \end{Bmatrix} \begin{Bmatrix} CAMXN33 \\ CAMYN33 \\ CAMZN33 \end{Bmatrix} = \begin{Bmatrix} 0 \\ 0 \\ 1 \end{Bmatrix} \tag{A-32}$$

Expanding the above matrices, and including only the equations with x_{11}, y_{12}, and z_{13}, yields

$$x_{11}CAMXN11 + y_{12}CAMYN11 + z_{13}CAMZN11 = 0 \tag{A-33}$$

$$x_{11}CAMXN22 + y_{12}CAMYN22 + z_{13}CAMZN22 = 0 \tag{A-34}$$

and

$$x_{11}CAMXN33 + y_{12}CAMYN11 + z_{13}CAMZN33 = 1 \tag{A-35}$$

Writing these equations in matrix form and solving for x_{11}, y_{12}, and z_{13}, there results

$$\begin{Bmatrix} x_{11} \\ y_{12} \\ z_{13} \end{Bmatrix} = \begin{Bmatrix} CAMXN11 & CAMYN11 & CAMZN11 \\ CAMXN22 & CAMYN22 & CAMZN22 \\ CAMXN33 & CAMYN33 & CAMZN33 \end{Bmatrix}^{-1} \begin{Bmatrix} GAX11 \\ GAX22 \\ GAX33 \end{Bmatrix} \tag{A-36}$$

Similarly,

$$\begin{Bmatrix} x_{21} \\ y_{22} \\ z_{23} \end{Bmatrix} = \begin{Bmatrix} CAMXN11 & CAMZN11 & CAMZN11 \\ CAMXN22 & CAMYN22 & CAMZN22 \\ CAMXN33 & CAMYN33 & CAMZN33 \end{Bmatrix}^{-1} \begin{Bmatrix} GAY11 \\ GAY22 \\ GAY33 \end{Bmatrix} \tag{A-37}$$

$$\begin{Bmatrix} x_{31} \\ y_{32} \\ z_{33} \end{Bmatrix} = \begin{Bmatrix} CAMXN11 & CAMZN11 & CAMZN11 \\ CAMXN22 & CAMYN22 & CAMZN22 \\ CAMXN33 & CAMYN33 & CAMZN33 \end{Bmatrix}^{-1} \begin{Bmatrix} GAX11 \\ GAX22 \\ GAX33 \end{Bmatrix} \tag{A-38}$$

The calibrated matrix serving to translate data from the axes of the separate accelerometers to the body axes and converting counts to g's, is comprised of terms from Eqs. (A-36) – (A-38):

$$\left[CTRNNB\right]^{-1} = \begin{Bmatrix} x_{11}y_{12}z_{13} \\ x_{21}y_{22}z_{23} \\ x_{31}y_{32}z_{33} \end{Bmatrix} \tag{A-39}$$

The matrix is not orthogonal because the elements represent gain factors and rotations for three independent accelerometers at three unique locations.

Although the development has been outlined for the forward (nose) accelerometer array, the procedure would be entirely similar for the accelerometer array in the aft (tail) region of the model.

NOMENCLATURE

A	Acceleration
a	Speed of sound, ft/sec
A/D	Analog-to-digital
B	Body
BL	Aircraft butt line, measured perpendicular to the longitudinal plane of symmetry of the aircraft, inches at model scale
C	Counts of instrument output, measured in a decimal fraction of volts
CG , cg	Center of gravity
D	Maximum diameter of the store model body, in.
DC	Direct current
DELPHI	Change in roll angle of the model between the initial, or captive position, and a given point in the trajectory, deg
DELPSI	Change in yaw angle of the model between the initial, or captive position, and a given point in the trajectory, deg
DELTHA	Change in pitch angle of the model between the initial, or captive position, and a given point in the trajectory, deg
FS	Aircraft fuselage station, measured along the centerline reference axis of the aircraft, inches at model scale
G	Designation for units of gravity
g	Acceleration of gravity at the earth's surface, assumed to be 32.174 ft/sec^2
I	Designation for the inertial axis system

I_{XX}	Moment of inertia of the model about the X_B axis, lb-in.^{2}
I_{XY}	Product of inertia of the model about the X_BY_B plane, lb-in.^{2}
I_{XZ}	Product of inertia of the model store about the X_BZ_B plane, lb-in.^{2}
I_{YY}	Moment of inertia of the model store about the Y_B axis, lb-in.^{2}
I_{YZ}	Product of inertia of the model store about the Y_BZ_B plane, lb-in.^{2}
I_{ZZ}	Moment of inertia of the model store about the Z_B axis, lb-in.^{2}
L	Length of the store model, in.
M_	Measured quantity
N	Designation for the nose region of the model
PHI	Roll angle of a store model about the X_B axis, deg
PSI	Yaw angle of a store model about the Z_B axis, deg
P	Rolling velocity of the store model, rad/sec
Q	Pitching velocity of the store model, rad/sec
R	Yawing velocity of the store model, rad/sec
T	Designation for the tail region of the model
TRN	Transfer matrix, transferring quantities from the point of detection to the model cg
t	Time, sec
W	Weight of the model, lb
X	Distance from the store nose, measured in the X_B direction, inches at model scale

X_{CG} Distance from the store nose, measured in the X_B direction, to the store cg, inches at model scale

Y_{CG} Distance from the longitudinal axis of the store model, measured in the Y_B direction, to the store cg, inches at model scale

Z_{CG} Distance from the longitudinal axis of the store model, measured in the Z_B direction, to the store cg, inches at model scale

$\dot{\theta}_m$ Pitch velocity imparted to the store by the ejector, deg/sec

Subscripts

N Nose

T Tail

t Quantity evaluated at time t

Pylon Axis System

Origin: Coincident with the projection of the store cg onto the longitudinal plane of symmetry of the pylon when the store was in the captive position. The pylon axes remained with the aircraft and translated along the flight path at the free-stream velocity. The axes rotated to maintain constant angular orientation with respect to the flight path direction.

Direction of the Axes:

X_p Parallel to the longitudinal axis of the store at release, and at a constant angular orientation with respect to the current flight path direciton, positive upstream.

Y_p Perpendicular to the X_p direction and parallel to the $X_F Y_F$ flight plane. The positive direction was out the right wing.

Z_p Perpendicular to the X_p and Y_p directions. The positive direction was away from the aircraft, downward as sensed by a pilot in upright flight.

Store Body Axis System

Origin: Coincident with the cg of the store at all times. Since the axes rotated with the store in pitch, yaw, and roll, the mass moments of inertia and products of inertia of the store were constant.

Direction of the Axes:

X_B Parallel to the longitudinal axis of the store, positive upstream at release of the store.

Y_B Perpendicular to the X_B and Z_B directions, positive to the right when looking upstream with the store at zero yaw and zero roll angles.

Z_B Perpendicular to the X_B direction and parallel to the plane of symmetry of the flat plate/cavity model when the store and aircraft models were at zero yaw and zero roll angles. The positive direction was downward as sensed by a pilot of the aircraft when the store was at zero pitch and zero roll angles.

Flight Axis System

Origin: Coincident with the origin of the Reference Axis System.

Direction of the Axes:

X_F Parallel to the direction of the flight path of the aircraft, positive downstream.

Y_F Perpendicular to the X_F and Z_F directions. The positive direction was out the right wing.

Z_F Parallel to the longitudinal plane of symmetry of the aircraft, and perpendicular to the aircraft flight path. The positive direction was away from the aircraft, downward as sensed by a pilot of the aircraft in an upright, level attitude.